NAA–SR–3762

327

MEASUREMENT OF ZERO POWER FREQUENCY RESPONSE OF THE SRE

AEC Research and Development Report

ATOMICS INTERNATIONAL

A DIVISION OF NORTH AMERICAN AVIATION, INC.

LEGAL NOTICE

Price $1.25
Available from the Office of Technical Services
Department of Commerce
Washington 25, D. C.

NAA–SR–3762
PHYSICS AND MATHEMATICS
58 PAGES

MEASUREMENT OF ZERO POWER FREQUENCY RESPONSE OF THE SRE

By
J. G. LUNDHOLM, JR.
C. W. GRIFFIN
E. R. MEISE

ATOMICS INTERNATIONAL
A DIVISION OF NORTH AMERICAN AVIATION, INC.
P.O. BOX 309 CANOGA PARK, CALIFORNIA

CONTRACT: AT(11–1)–GEN–8
ISSUED: NOV 1 1960

DISTRIBUTION

This report has been distributed according to the category "Physics and Mathematics" as given in "Standard Distribution Lists for Unclassified Scientific and Technical Reports" TID-4500 (15th Ed.), August 1, 1959. A total of 655 copies was printed.

ACKNOWLEDGMENT

The authors are greatly indebted to many persons for their contributions to this project. Members of the Experimental Unit of the SRE spent many hours setting up equipment, assisting with the experimental measurements, and analyzing data. The efforts and patience of the Reactor Operations Unit are especially acknowledged. The many technical contributions from and helpful discussions with Mr. E. B. Ash are gratefully acknowledged.

CONTENTS

		Page
	Abstract	vi
I.	Introduction	1
II.	Derivation of Linearized Reactor Transfer Function	2
III.	Derivation of Reactor Transfer Function Considering Feedback Effects	8
	A. Control System Feedback Theory	8
	B. Treatment of Delayed Neutrons as a Feedback Effect	9
	C. Delayed Neutron Parameters for the SRE	10
	D. Power Feedback Effects and Power Coefficients	12
	E. Introduction to Reactor Transfer Function Measurements	14
IV.	Equipment for Obtaining Sinusoidal Variations of Reactivity	16
	A. Requirements	16
	B. Types of Reactivity Mechanisms Employed for SRE Tests	17
	1. Rotary Device	18
	2. Scotch-Yoke Device	23
	3. Direct Drive Device	26
	C. Mechanical Drive Mechanism	27
V.	Measurement of Reactor Transfer Functions	29
	A. Requirements	29
	B. Methods	29
	1. Direct Visual Method	30
	2. Quadrature Component Method	30
	3. Null-Balance Method	31
	C. Instrumentation	31
	1. Neutron Detectors	31
	2. Electrometer	31
	3. Correlation Equipment	33
	4. Sine-Cosine Potentiometers	35
	5. Servo Plate Details	36

CONTENTS

		Page
	D. Special Equipment for "At Power" Measurements	38
VI.	Experimental Techniques and Analysis of Data	39
	A. Introduction	39
	B. Measurements Utilizing Rotary Device and Correlation Equipment	39
	C. Analysis of Data	42
VII.	Interpretation of Experimental Results	44
VIII.	Summary and Conclusions	45
	Appendix. Development of Correlation Measurement Theory and Method	46
	References	52

TABLES

I.	Delayed Neutron Group Constants for U^{235}	12
II.	Reactor Gain vs Frequency	16
III.	Advantages and Disadvantages of Three Reactivity Varying Mechanisms	18
IV.	Comparison of the Three Methods for Measuring Reactor Transfer Function, Gain, and Phase Angle	30

FIGURES

1.	Block Diagram of Reactor With Feedback Transfer Function	8
2.	Block Diagram of Techniques for Treating Delayed Neutrons as a Feedback Mechanism	11
3.	Block Diagram of $G(s)_P$ Showing Reactivity Feedback Mechanisms	13
4.	Rotor and Stator of Rotary Sinusoidal Reactivity Device	19
5.	Boral Poison Squares Mounted on Rotor and Stator of Rotary Sinusoidal Reactivity Device	19

Page

6. Reactivity Waveform of Rotary Sinusoidal Reactivity Device 20
7. Cross Section of Rotary Sinusoidal Reactivity Device Showing Location and Dimensions of Poison Squares 21
8. Relative Sizes of Rotor and Stator Squares 21
9. Theoretical Shape of Rotor Poison Square 21
10. Scotch-Yoke Gear Box for Driving Control Rod Ball-Nut-Screw Mechanism With a Sinusoidal Motion 23
11. Scotch-Yoke Gear Box and Correlation Sine-Cosine Potentiometers in use With the Oscillator Drive Mechanism at the SRE 25
12. Special DC Motor Drive and Gear Boxes 27
13. Entire Oscillator Mechanism in use During Oscillation Measurements at the SRE 28
14. Oscillation Measurement Equipment Consisting of Recording Oscillographs, Operational Amplifiers, Electrometer, and Control Circuits 32
15. Circuit Layout for Correlation Measurements 33
16. Typical Oscillograph Record of Reactor Tests Employing Scotch-Yoke Reactivity Device 34
17. Typical Oscillograph Record of Reactor Tests Employing Direct Drive Reactivity Device 35
18. Servoplate Containing Sine-Cosine Potentiometers and Phase Adjusting Differentials Employed for Correlation Measurements 37
19. Circuit Layout for Oscillation Temperature Measurement With Correlation Methods 38
20. Typical Oscillograph Record of Reactor Tests Employing Rotary Device 41
21. SRE Zero Power Transfer Function 43

ABSTRACT

This report describes the derivation of both the zero power linearized reactor transfer function, and the transfer function with feedback due to power and temperature effects in the core. The instrumentation and special techniques used to measure these transfer functions are also described.

The zero power frequency response function measurements on the SRE confirmed the experimental methods employed. The experimental data correlated quite well with the linearized zero power reactor transfer function, and the measurements provided an experimentally determined value of ℓ/β,

I. INTRODUCTION

The usefulness of transfer function or frequency response measurements on nuclear reactors has become increasingly evident in the last few years. There is a large volume of fundamental theory available in this area, and the merits of this type of measurement are well known in the fields of servo-mechanisms and feedback control systems.

For nuclear reactors, the technique is useful both for determining stability characteristics and nuclear parameters. With this method, (1) the power coefficient of reactivity may be measured, (2) control rod calibrations may be determined, and (3) the magnitude and response time of the temperature coefficients of reactivity are obtainable.

II. DERIVATION OF LINEARIZED REACTOR TRANSFER FUNCTION

The theoretical reactor transfer function will now be derived. The starting point for the derivation of this transfer function is, as usual, the basic differential equations of the process. Since one of the differential equations involves a product of two variables, which are both functions of time, it must be considered a nonlinear differential equation. For this reason, it is necessary to linearize the equations before taking the Laplace transform of them in preparation to placing them in the usual transfer function form. Because of the linearization process, the resultant transfer function is suitable only for small variations of the variables. This transfer function will not be suitable for large step inputs or transient studies. It is, however, perfectly adequate for frequency response studies where changes in a variable are held to a few percent variation about its equilibrium value.

The basic kinetic differential equations for a nuclear reactor are as follows:

$$\frac{dn(t)}{dt} = \frac{\rho(t)n(t)}{\ell} - \frac{\beta}{\ell}n(t) + \Sigma\lambda_i C_i(t) \qquad \ldots(1)$$

$$\frac{dC_i(t)}{dt} = \frac{\beta_i}{\ell}n(t) - \lambda_i C_i(t) \ , \qquad \ldots(2)$$

where

$n(t)$ = neutron flux or power level

t = time

$\rho(t)$ = reactivity input to reactor

β = total effective fraction of all neutrons which are born as delayed neutrons

β_i = effective fraction of delayed neutrons in the i^{th} group,

where $\sum_{i=1}^{6} \beta_i = \beta$

ℓ = effective neutron lifetime

λ_i = decay constant for delayed neutrons in the i^{th} group. $1/\lambda_i$ is the mean lifetime of delayed neutrons in the i^{th} group

$C_i(t)$ = concentration of delayed neutrons in the i^{th} group

If there was not the product term $\rho(t)n(t)$ in the first equation, one would immediately Laplace transform both equations, eliminate C(s) between them, and place them in the desired transfer function form giving $n(s)/\rho(s)$. Due to the product term, it will be necessary to linearize the first equation. The results will be written in terms of $\delta n(s)$ and $\delta\rho(s)$, indicating that the final equation is suitable only for small changes in n(s) and $\rho(s)$.

The usual process of linearization is to substitute for the variables n(t), $\rho(t)$, and C(t), as follows:

$$n(t) = n_o + \delta n(t) \quad , \qquad \ldots(3)$$

$$\rho(t) = \rho_o + \delta\rho(t) \quad , \qquad \ldots(4)$$

$$C(t) = C_o + \delta C(t) \quad , \qquad \ldots(5)$$

where n_o, ρ_o, and C_o are the equilibrium or steady state values of the original variables, and $\delta n(t)$, $\delta\rho(t)$, and $\delta C(t)$ represent the small changes in the variables as a function of time. This is identical to the usual method of determining electron tube parameters and analyzing electron tube circuits.

We now substitute the above linearizing equations into the basic reactor kinetic Equations 1 and 2.

$$\frac{d}{dt}\left[n_o + \delta n(t)\right] = \frac{\left[\rho_o + \delta\rho(t)\right]\left[n_o + \delta n(t)\right]}{\ell} - \frac{\beta}{\ell}\left[n_o + \delta n(t)\right] + \sum_{i=1}^{6} \lambda_i \left[C_o + \delta C_i(t)\right] \qquad \ldots(6)$$

and

$$\frac{d}{dt}\left[C_o + \delta C_i(t)\right] = \frac{\beta_i}{\ell}\left[n_o + \delta n(t)\right] - \lambda_i\left[C_o + \delta C_i(t)\right] \quad . \qquad \ldots(7)$$

On expanding, assuming second order terms such as $\delta n(t)\delta\rho(t)$ are negligible in value, and subtracting the equilibrium values from the above equations, the results are as follows:

$$\frac{d}{dt}\,\delta n(t) = \frac{n_o}{\ell}\delta\rho(t) - \frac{\beta}{\ell}\delta n(t) + \sum_{i=1}^{6} \lambda_i \delta C_i(t) \qquad \ldots(8)$$

and

$$\frac{d}{dt}\delta C_i(t) = \frac{\beta_i}{\ell}\delta n(t) - \lambda_i \delta C_i(t) \quad . \qquad \ldots(9)$$

Normally, ρ_o has the value of zero. This means that the variation in ρ, which is $\delta\rho(t)$, is about the critical point, $\rho_o = 0$. To a first approximation, this also means that the average power or flux, n_o, will stay constant with time, if the variation is sinusoidal.

Taking the Laplace transform of Equations 8 and 9 gives

$$s\,\delta n(s) = \frac{n_o}{\ell}\delta\rho(s) - \frac{\beta}{\ell}\,\delta n(s) + \sum_{i=1}^{6} \lambda_i \delta C_i(s) \qquad \ldots(10)$$

and

$$s\,\delta C_i(s) = \frac{\beta_i}{\ell}\delta n(s) - \lambda_i \delta C_i(s) \qquad \ldots(11)$$

From Equation 11,

$$\frac{\delta C_i(s)}{\delta n(s)} = \frac{\beta_i/\ell}{s + \lambda_i} \quad . \qquad \ldots(12)$$

Substituting Equation 12 into Equation 10,

$$s\delta n(s) = \frac{n_o}{\ell}\,\delta\rho(s) - \frac{\beta}{\ell}\delta n(s) + \delta n(s) \sum_{i=1}^{6} \frac{\lambda_i \beta_i/\ell}{(s + \lambda_i)} \quad . \qquad \ldots(13)$$

Collecting terms, and rearranging gives

$$\frac{\delta n(s)}{\delta\rho(s)} = \frac{n_o}{\ell\left(s + \beta/\ell - \sum_{i=1}^{6} \frac{\lambda_i \beta_i/\ell}{s + \lambda_i}\right)} \quad . \qquad \ldots(14)$$

On letting $\beta/\ell = \Sigma\beta_i/\ell$, and placing it inside the summation sign of the third term in the denominator, forming a common denominator, and, clearing terms, the desired transfer function is obtained.

$$\frac{\delta n(s)}{\delta\rho(s)} = \frac{n_o}{s\ell\left[1 + \sum_{i=1}^{6} \frac{\beta_i/\ell}{\ell(s + \lambda_i)}\right]} \quad . \qquad \ldots(15)$$

The above transfer function may be placed into a normalized form to eliminate its dependence on reactor power, n_o, and employ ℓ/β as a parameter. The following equation is thus obtained:

$$\frac{\frac{\delta n(s)}{n_o}}{\frac{\delta \rho(s)}{\beta}} = \frac{1}{s\frac{\ell}{\beta}\left[1 + \sum_{i=1}^{6} \frac{\beta_i/\beta}{(\ell/\beta)(s + \lambda_i)}\right]} \quad . \qquad \ldots(16)$$

It is possible to further manipulate Equation 15 into other useful forms. The bracketed term in the denominator can be rearranged to have a common denominator as follows:

$$\left[1 + \sum_{i=1}^{6} \frac{\beta_i}{\ell(s + \lambda_i)}\right] = 1 + \frac{\beta_1}{s + \lambda_1} + \frac{\beta_2}{s + \lambda_2} + - - - + \frac{\beta_6}{s + \lambda_6} \qquad \ldots(17)$$

$$= \frac{(s + \lambda_1)(- - -)(s + \lambda_6) + \beta_1 (s + \lambda_2) - - - (s + \lambda_6) + - - -}{(s + \lambda_1) - - - (s + \lambda_6)} \qquad \ldots(18)$$

$$= \frac{\prod_{k=1}^{6} (s + \alpha_k)}{\prod_{i=1}^{6} (s + \lambda_i)} \quad , \qquad \ldots(19)$$

where the α_k's are the roots of the numerator of Equation 18.

This technique will give a transfer function form as follows:

$$\frac{\delta n(s)}{\delta \rho(s)} = \frac{n_o}{s\ell} \frac{\prod_{i=1}^{6} (s + \lambda_i)}{\prod_{k=1}^{6} (s + \alpha_k)} \quad . \qquad \ldots(20)$$

This isolates the poles and zeros of the transfer function and allows one to plot the magnitude and phase values of the transfer function by the usual approximation methods.

Figure 21, p 43 shows the Bode plot of the theoretical, linearized reactivity transfer function. It is important to note that the absolute gain of the transfer function is directly proportional to n_o, the flux or power level of the reactor. It may be necessary to automatically decrease the sensitivity of the controller in the flux control loop of a reactor as the reactor power level increases – in order to obtain the same degree of control and prevent oscillations in power due to excessive loop gain.

It will be necessary to consider the effects of the linearization process, namely how large a variation in $\delta\rho(t)$ and $\delta n(t)$ is allowable before the results depart from the derived linearized transfer function. This is not a simple calculation but some work has been done to study the effect.[1] One other major consequence of using large sinusoidal variation in $\delta\rho(t)$ is that the average reactor power will increase slowly. The in-hour equation shows that the positive periods obtained are shorter than negative periods – for a given reactivity change. These items will be covered in more detail later when the techniques and problems associated with experimentally measuring the transfer function are discussed.

III. DERIVATION OF REACTOR TRANSFER FUNCTION CONSIDERING FEEDBACK EFFECTS

A. CONTROL SYSTEM FEEDBACK THEORY

The basic feedback control system equation will now be derived. It will be needed to determine the effects of temperature coefficients of reactivity on the zero power reactor transfer function. Temperature coefficients, along with xenon poisoning, are examples of a power feedback effect, and either add or subtract from the direct reactivity input or forcing signal. It will also show the manner in which delayed neutrons may be considered as a feedback effect.

The basic block diagram for a feedback control system is shown in Figure 1.

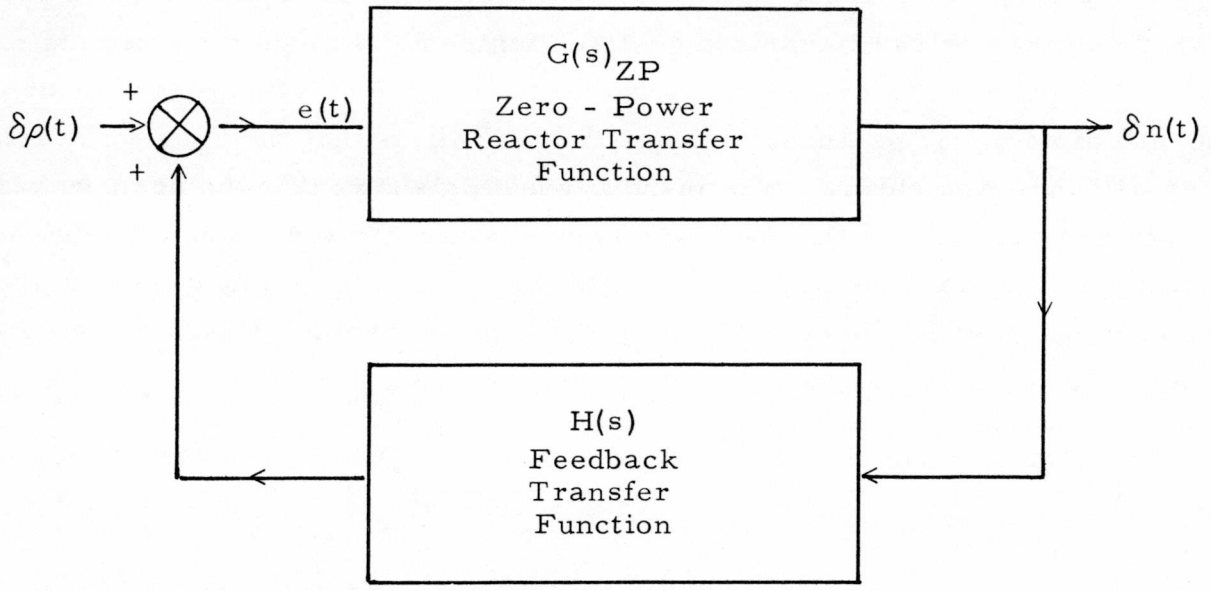

Figure 1. Block Diagram of Reactor With Feedback Transfer Function

$\delta\rho(t)$ = reactivity input signal

$\delta n(t)$ = power variation of reactor

e (t) = error signal to reactor; sum of input reactivity signal and reactivity feedback effects

The basic derivation is as follows:

$$e(t) = \delta\rho(t) + H(s)\delta n(t) , \qquad \ldots(21)$$

and

$$\delta n(t) = e(t)G(s)_{ZP} \quad . \qquad \ldots(22)$$

Eliminating $e(t)$ from Equations 22 and 23, and rearranging, gives the fundamental feedback theory equation

$$G(s)_p = \frac{\delta n(t)}{\delta \rho(t)} = \frac{G(s)_{ZP}}{1 - G(s)_{ZP}H(s)} \quad , \qquad \ldots(23)$$

where $[G(s)]_{ZP}$ is the zero power - linearized reactor transfer function derived in Section II. $[G(s)]_p$ represents the overall reactor transfer function when there are reactivity feedback effects due to power or temperatures.

B. TREATMENT OF DELAYED NEUTRONS AS A FEEDBACK EFFECT

The zero power linearized reactor transfer function is rearranged to treat the effect of delayed neutrons as a feedback mechanism. This will be done mainly to provide additional insight into feedback effects. Many digital codes for reactor kinetics actually operate on this basis.

Referring to Equation 10,

$$s\delta n(s) = \frac{n_o}{\ell}\,\delta\rho(s) - \frac{\beta}{\ell}\,\delta n(s) + \sum_{i=1}^{6} \lambda_i\,\delta C_i(s) \quad . \qquad \ldots(10)$$

Rearranging,

$$\delta n(s) = \frac{n_o}{\ell(s + \beta/\ell)}\,\delta\rho(s) + \sum_{i=1}^{6} \frac{\lambda_i}{(s + \beta/\ell)}\,\delta C_i(s) \quad . \qquad \ldots(24)$$

Also,

$$\delta C_i(s) = \delta n(s) \frac{\beta_i/\ell}{s + \lambda_i} . \qquad \ldots(12)$$

Figure 2, Step 1, shows the results of Equations 24 and 12 in block diagram form.

Figure 2, Step 2, is the final desired block diagram. It shows the delayed neutron groups as a feedback mechanism. The forward block,

$$\frac{n_o}{\ell\left(s + \frac{\beta}{\ell}\right)} ,$$

represents the reactor transfer function at the higher frequencies where delayed neutron effects are no longer important.

Although it would be possible to separate the delayed neutrons as shown above, they will not be separated in the rest of this work. $G(s)_{ZP}$ will be used to represent the zero power linearized reactor transfer function. $G(s)_P$ will represent the transfer function at other than zero power, indicating that power and temperature feedback effects are operating.

C. DELAYED NEUTRON PARAMETERS FOR THE SRE

Table I lists the delayed neutron data used for all analysis on the SRE. From this table, it can be seen that the delayed neutron group with the highest break frequency is the sixth group whose break frequency is 0.617 cycles per second. At this frequency, its effects are already down 3 db, or 0.707 of its dc value. At ten times this frequency, the effects of this group can be ignored.

Even the prompt neutron group will be unable to follow sufficiently high sinusoidal frequencies. This break frequency is given by β/ℓ, and for the SRE is 2.13 cps; where $\beta = 0.007$, and $\ell = 5.25 \times 10^{-4}$ seconds. It is interesting to note that this frequency is only 3.5 times the break frequency of the sixth life delayed neutron group. Simple calculations have shown that since the fraction of delayed neutrons in this long life group is so small, it has little effect on the transfer function near the prompt neutron break frequency point.

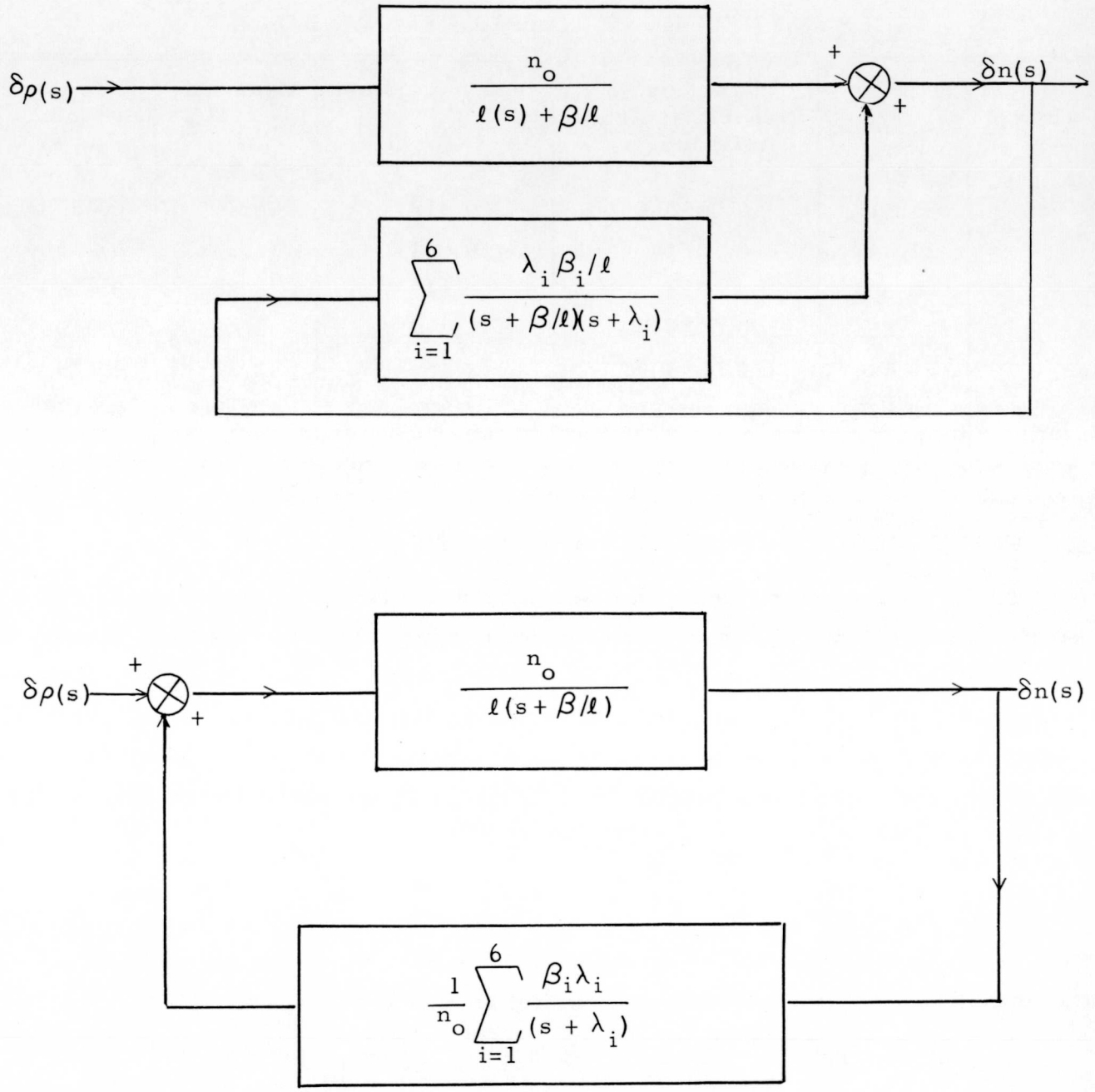

Figure 2. Block Diagram of Techniques for Treating Delayed Neutrons as a Feedback Mechanism

TABLE I

DELAYED NEUTRON GROUP CONSTANTS FOR U^{235}*

Group	Half-life $T_{1/2}$ (sec)	Fraction of Delayed Neutrons in Group, β_i	Decay Constant λ_i (sec^{-1})	Mean Life $\tau_i = 1/\lambda_i$ (sec)	Break Frequency (cps)
1	54.51	0.000264	0.0127	78.8	0.00202
2	21.84	0.00149	0.0317	31.6	0.00504
3	6.00	0.00132	0.115	8.70	0.0183
4	2.23	0.00285	0.311	3.22	0.0495
5	0.496	0.000895	1.40	0.715	0.223
6	0.179	0.000182	3.87	0.258	0.617

*Data from G. R. Keepin and T. F. Wimett, Nucleonics 16, (10) (1958) p 86

D. POWER FEEDBACK EFFECTS AND POWER COEFFICIENTS

The most important feedback mechanisms are those of temperature coefficients of reactivity and xenon-samarium poisoning. In some reactors, such as homogeneous and boiling water, void formation would represent another important power feedback mechanism. In this report only temperature coefficients of reactivity will be considered. The frequency response of xenon poisoning is in the order of a cycle per day, and thus can be ignored from the reactor stability standpoint.

Figure 3, is a block diagram of the reactor "at power" transfer function $G(s)_p$ and shows the predominant reactivity feedback mechanisms, as well as the fuel and moderator temperature coefficients of reactivity.

In equation form, one obtains

$$G(s)_P = \frac{\delta n(s)}{\delta \rho(s)} = \frac{G(s)_{ZP}}{1 - G(s)_{ZP}\left(\bar{\alpha}_f \frac{\delta \bar{T}_f(s)}{\delta n(s)} + \bar{\alpha}_m \frac{\delta \bar{T}_m}{\delta n(s)} \right)} \qquad \ldots(25)$$

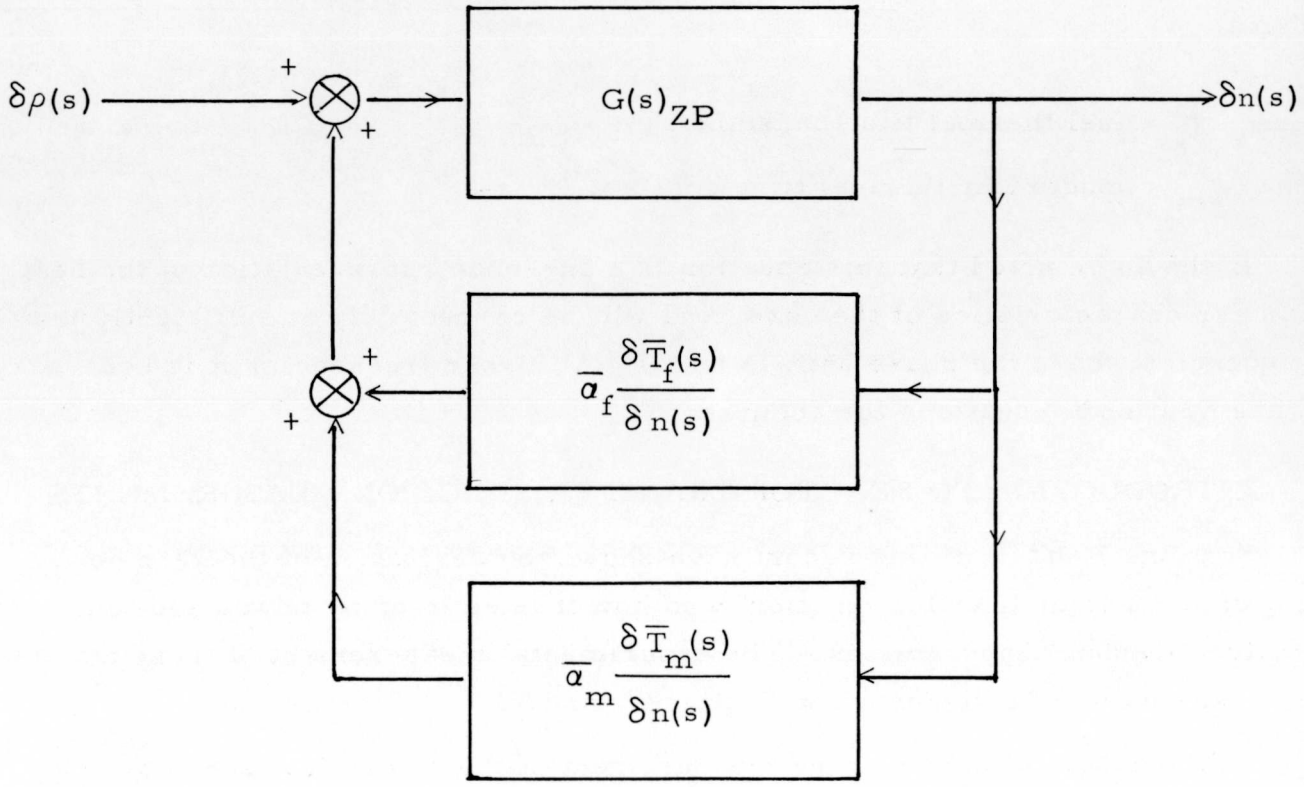

Figure 3. Block Diagram of $G(s)_P$ Showing Reactivity Feedback Mechanisms

where

$\delta \overline{T}_f(s)$ = small variation in average fuel temperature

$\delta \overline{T}_m(s)$ = small variation in average moderator temperature

$\overline{\alpha}_f$ = average fuel temperature coefficient of reactivity per °F

$\overline{\alpha}_m$ = average moderator temperature coefficient of reactivity per °F.

Equation 25 may also be written

$$G(s)_P = \frac{G(s)_{ZP}}{1 - G(s)_{ZP}\left[\overline{\alpha}_f \frac{|\delta \overline{T}_f / \delta n|}{(1 + s\,\tau_f)} + \overline{\alpha}_m \frac{|\delta \overline{T}_m / \delta n|}{(1 + s\,\tau_m)}\right]} , \qquad \ldots(26)$$

where

τ_f = fuel thermal time constant

τ_m = moderator thermal time constant.

It should be noted that this equation is a one-node representation of the heat transfer characteristics of the core, and will be correct only at sufficiently low frequencies where the phase shift is small. At higher frequencies it is necessary to use multinode equations for accuracy.

E. INTRODUCTION TO REACTOR TRANSFER FUNCTION MEASUREMENTS

Sections II and III of this report have shown the derivation of the zero power, linearized reactor transfer function, and how it is effected by power and temperature feedback mechanisms. The experimental measurement of these transfer functions will be discussed in Sections V and VI.

It is possible to consider the measurement of the theoretical zero power transfer function $G(s)_{ZP}$ from two standpoints, (1) verifying the theory, and (2) checking the experimental techniques. From the many problems encountered in making accurate magnitude and phase measurements in the frequency range of 0.0005 to 20 cps, it is believed that viewpoint 2 is preferable. If consistent results can be obtained that check within ±5% for the magnitude, and within 1° or 2° for the phase of the theoretical transfer function, then sufficient confidence can be placed in the transfer function measurements at power.

To verify the operation of the equipment and techniques, a number of tests were performed with the SRE. The results are discussed in detail in Section VII of this report. The oscillator was also employed to obtain control rod calibrations for the purpose of comparing this technique with the rod-bump-period method of calibrating rods.

To determine the power coefficient of reactivity H(s), it is necessary to know both the "at power" and zero power transfer functions, since the power coefficient is defined as follows:

$$H(s) = \frac{1}{G(s)_P} - \frac{1}{G(s)_{ZP}} \qquad \ldots(27)$$

Since H(s) is the difference between two quantities which are nearly equal, it is necessary to measure $G(s)_P$ and $G(s)_{ZP}$ as accurately as possible. This accounts for the large effort expended on instrumentation and correlation techniques. At the same time, many other facets of this problem must be considered, such as the method of varying reactivity, magnitude and waveform of reactivity variation, linearities, and accuracies of various instruments. These will all be discussed later in this report.

IV. EQUIPMENT FOR OBTAINING SINUSOIDAL VARIATIONS OF REACTIVITY

A. REQUIREMENTS

An optimum reactivity varying mechanism would produce a perfect sine wave variation of reactivity at all necessary frequencies and have provision for selecting the magnitude of the reactivity variation. For the SRE measurements, the part of the mechanism located in the reactor would have to operate in temperatures of at least 1000°F and a thermal neutron flux of up to 6×10^{13} nv.[3]

It was desirable to vary reactivity over a frequency range of 0.0005 to 20 cps for the zero power tests and from 0.0005 to 1 cps for the power tests. At low frequency, the gain of a reactor increases inversely to the frequency of oscillation, making it difficult to select an optimum magnitude of reactivity variation if a constant reactivity variation must be used.

Table II shows the value of reactivity variation which will produce a 5% change in power, and the percent change in power for a constant reactivity magnitude variation of $5 \times 10^{-5} \delta\rho$ — both as a function of the forcing frequency. The gain of the reactor is also shown as a function of frequency.

TABLE II

REACTOR GAIN VS FREQUENCY

($\delta n/n$ vs $\delta\rho$, and $\delta\rho$ for a given $\delta n/n$ for various frequencies)*

Frequency (cps)	Reactor Gain			$\delta n/n$ % for $\delta\rho = 5 \times 10^{-5}$	$\delta\rho$ for $\delta n/n = 5\%$
	$20 \log \frac{\delta n}{n_o \delta\rho/\beta}$ †	$\frac{\delta n}{n_o \delta\rho/\beta}$	$\frac{\delta n}{n_o \delta\rho}$		
0.0005	27.82	24.6	3510	17.5	0.14×10^{-4}
0.001	22.08	12.7	1810	9.1	0.28×10^{-4}
0.01	8.36	2.62	374	1.8	1.34×10^{-4}
0.1	1.43	1.18	168	0.84	2.98×10^{-4}
1	-1.00	0.892	127	0.64	3.93×10^{-4}
10	13.6	0.209	29.8	0.15	16.8×10^{-4}
20	19.45	0.108	15.4	0.08	32.4×10^{-4}

*δn and $\delta\rho$ are sine wave magnitude values
†decibel units

The optimum choice for the magnitude of reactivity variation depends on two important considerations: (1) the minimum value of $|\delta n/n|$ that can be measured with sufficient accuracy – with instrumentation noise being present; and (2) the maximum value of $|\delta n/n|$ that can be allowed without errors appearing – because of the use of linearized, small signal theory in the derivation of the reactor transfer function. For this work, the minimum value of $|\delta n/n|$ that can be reliably measured with correlation techniques is 0.1%. The maximum value of $|\delta n/n|$, to stay within the accuracy of the linear equations, was taken to be 5%, where $|\delta n|$ is the magnitude of the sine wave variation of $\delta n \sin \omega t$. Actual measurements indicate that this value was very conservative.

One other important consideration is that the addition of equal amounts of positive and negative reactivity produce different reactor periods – the effect increasing with the magnitude of $\delta\rho$. This effect causes the average power level of the reactor to increase slowly during oscillation unless a very small negative reactivity change is made to the reactor at the start of oscillation. Performing exact correction at low frequencies is difficult. The drift in average power level may also be decreased by holding $|\delta n/n|$ to the smallest possible value. The drift is very troublesome on the low frequency tests, since it takes a long time to determine if the average power level is holding steady from one cycle to the next. With sinusoidal peaks being up to thirty minutes apart, an idea of the time consumed in stabilizing the reactor can be appreciated.

It can be seen from Table II that a value of $\delta\rho \approx 10^{-4}$ will produce a $|\delta n/n|$ of 0.15% at 20 cps, and of 18.1% at 0.001 cps. A value of $\delta\rho \approx 10^{-5}$ will produce $|\delta n/n|$ of 0.127% at 1.00 cps, and of 3.5% at 0.0005 cps. δn and $\delta\rho$ are sine wave magnitude values.

It can be seen that a method of obtaining various $\delta\rho$ magnitudes will be necessary in order to meet the original specifications. A discussion of the various types of reactivity mechanisms tested will now be given.

B. TYPES OF REACTIVITY MECHANISMS EMPLOYED FOR SRE TESTS

Three types of reactivity varying mechanisms were tested during the SRE oscillation experiments. These are listed as follows:

1) rotary device
2) Scotch-yoke (slider crank) mechanism to drive a shim rod

3) direct drive of shim rod by existing servo motor actuated by special sine wave tracking servo loop

Table III lists the advantages and disadvantages of each of these three devices. These various reactivity devices will now be individually discussed.

TABLE III

ADVANTAGES AND DISADVANTAGES OF THREE REACTIVITY VARYING MECHANISMS

Type	Advantage	Disadvantage
Rotary	1. High Frequency (20 cps)	1. Difficult to vary magnitude of $\delta\rho$
Scotch-Yoke	1. Testing at power 2. No change required in reactor loading	1. Possible mechanical backlash 2. Limited to $\approx$0.1 cps maximum
Direct Drive	1. Uses existing control system	1. Extra servo loop phase alignment 2. Limited to $\approx$0.1 cps maximum

1. Rotary Device

It was originally thought that this type of reactivity varying mechanism would be the best for the SRE measurements. Although two devices with different $\delta\rho$ magnitude would be necessary, this presented no difficulty because the devices could be handled by the SRE fuel handling cask – a straight forward operation. With the rotary device, any frequency from the lowest necessary up to 20 cps could be obtained. Figures 4 and 5 are views of the boral squares fastened to the aluminum rotor and stator of the rotary device. As the rotor turns, the boral or poison squares are alternately shielded by the stator poison squares and then exposed to the neutron flux. The resulting reactivity waveform is very close to a sine wave, as seen in Figure 6. With four poison squares 90° apart, four sine wave cycles of reactivity changes are obtained for one mechanical rotation of the rotor. Thus 20 cps of $\delta\rho$ variation requires 300 rpm for the rotor. The rotor was satisfactorily operated at speeds to 300 rpm (20 cps) during zero power tests and frequency response data were obtained.

The rotary device was designed to fit inside a spare SRE control rod thimble that had an inside diameter of 2.522 in. Schedule 40 aluminum pipe was selected for the stator and 1.75 in. diameter aluminum rod was selected for the rotor. Aluminum was selected for the test device because of its low thermal neutron

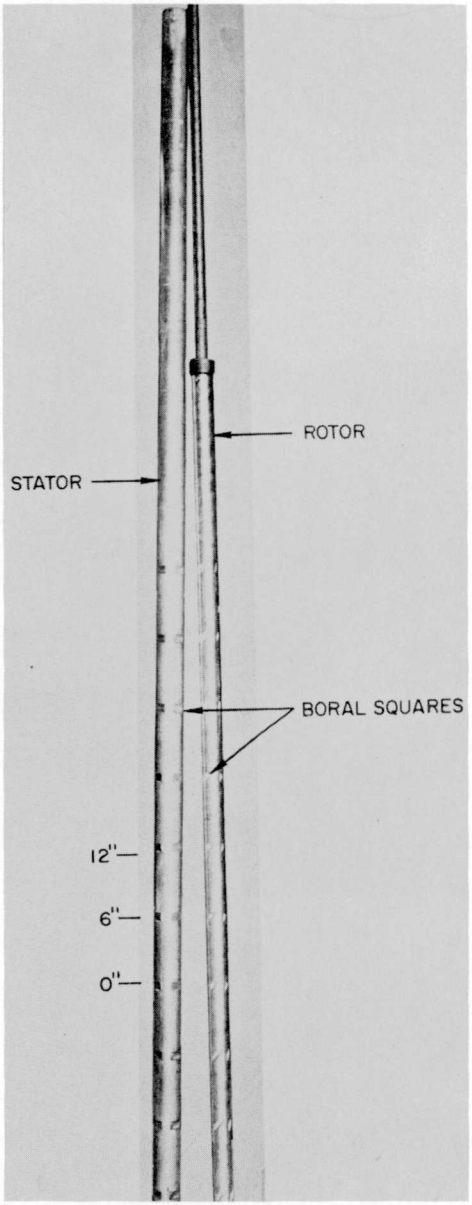

Figure 4. Rotor and Stator of Rotary Sinusoidal Reactivity Device

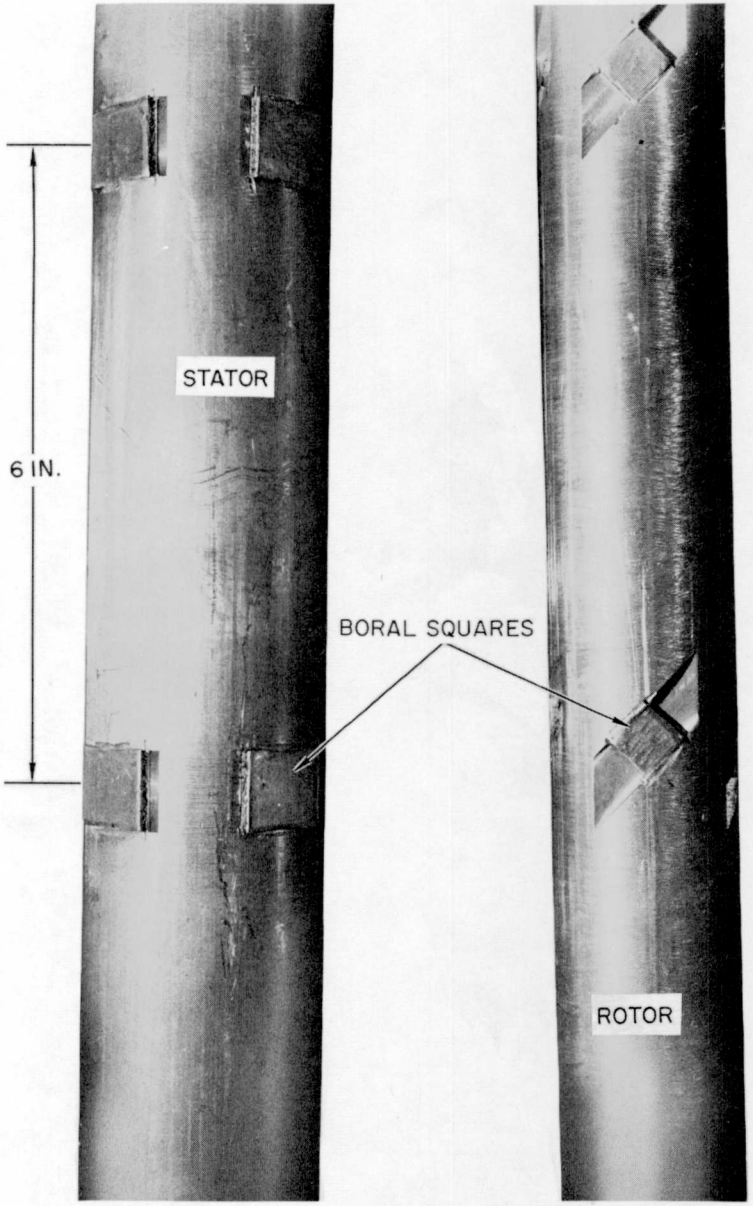

Figure 5. Boral Poison Squares Mounted on Rotor and Stator of Rotary Sinusoidal Reactivity Device

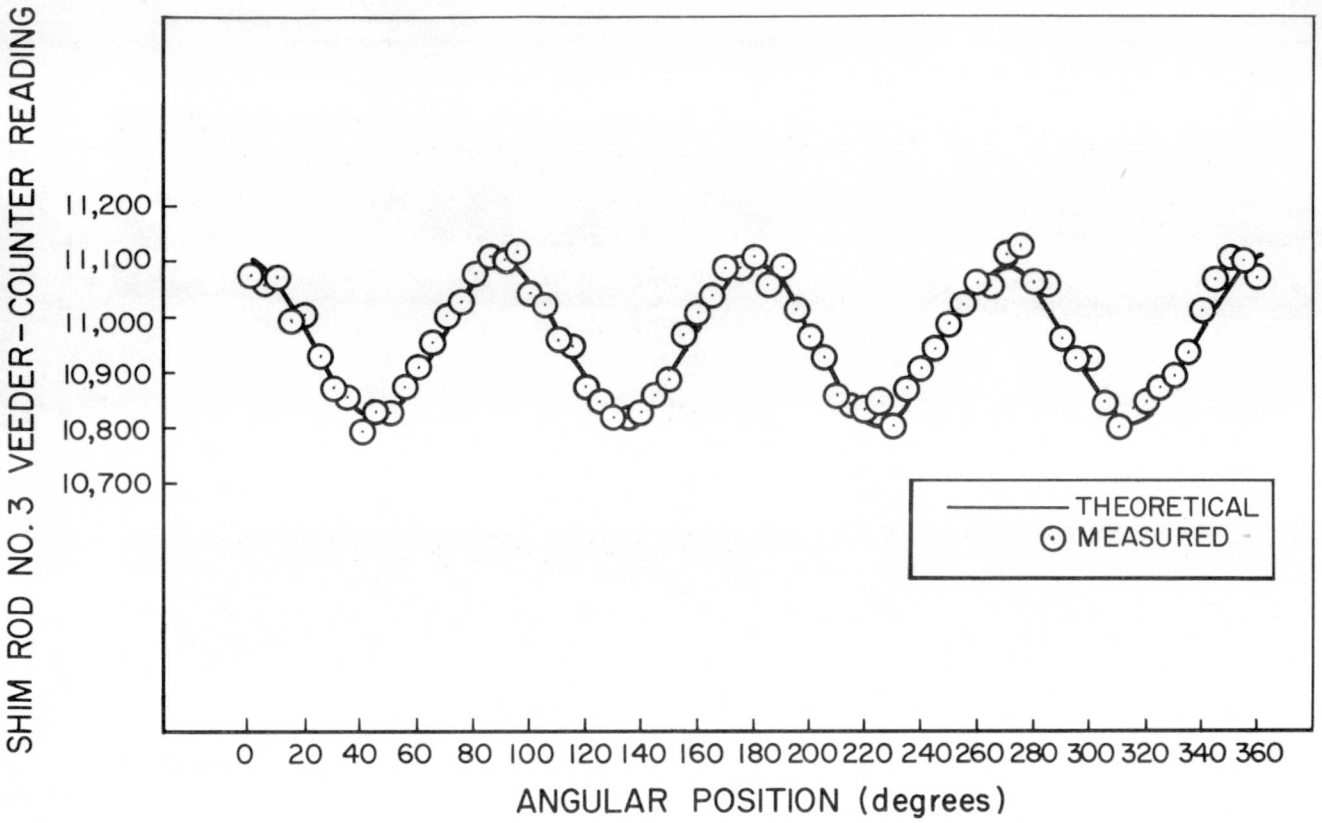

Figure 6. Reactivity Waveform of Rotary Sinusoidal Reactivity Device

capture cross section, and its availability. Boral was likewise chosen because of its availability and suitability for the test device.

Calculations of the heating effect in the rotor and stator due to the (n, α) reaction in boron and gamma heating in the aluminum showed that the rotor would operate 50°F/Mw above the temperature of the sodium surrounding the thimble. This would limit the use of the aluminum rotary device to a reactor power of approximately 1 Mw at a sodium outlet temperature of 600°F.

The next step in the design, after choosing the dimensions of the rotor and stator, was the determination of the dimensions and number of poison squares required to produce a reactivity variation of approximately 5% of β.

Figure 7 shows a cross section of the rotor and stator with poison squares. Due to shadowing effect uncertainties, the criteria chosen for the design were: (1) to size the rotor and stator squares to fit inside lines 1 and 2 when opposite each other; and (2) to fit between lines 2 and 3 when the rotor square was fully exposed and producing the maximum neutron poisoning effect. Figure 8 shows

the relative sizes of the rotor and stator poison squares. Although a mathematically correct shape for the rotor poison might be that shown in Figure 9, a simple square shape was used and found satisfactory.

Simple calculations indicated that two to four sets of squares would be necessary to achieve the desired reactivity change. The rotor and stator were milled to hold nine sets of chips. Since the sets are easier to remove than install, when the rotor becomes radioactive, four sets were installed initially, 6 in. apart, at the center positions on the rotor and stator.

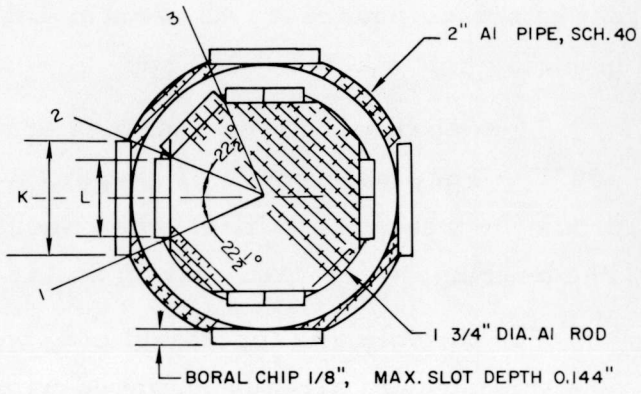

$L = (1.75/2 - 0.144)\ \text{TAN}\ 22.5° = 0.606" = 5/8"\ (\text{APPROX})$

$K = (2.375/2 - 0.144)\ \text{TAN}\ 22.5° = 0.866" = 7/8"\ (\text{APPROX})$

$Z^2 = (5/16)^2 + (5/16)^2 \quad Z = 15/32"$

Figure 7. Cross Section of Rotary Sinusoidal Reactivity Device Showing Location and Dimensions of Poison Squares

The value of reactivity variation produced by four sets of poison squares was 1.7×10^{-4} peak to peak. Although this value was four times larger than desired, it was unnecessary to remove a

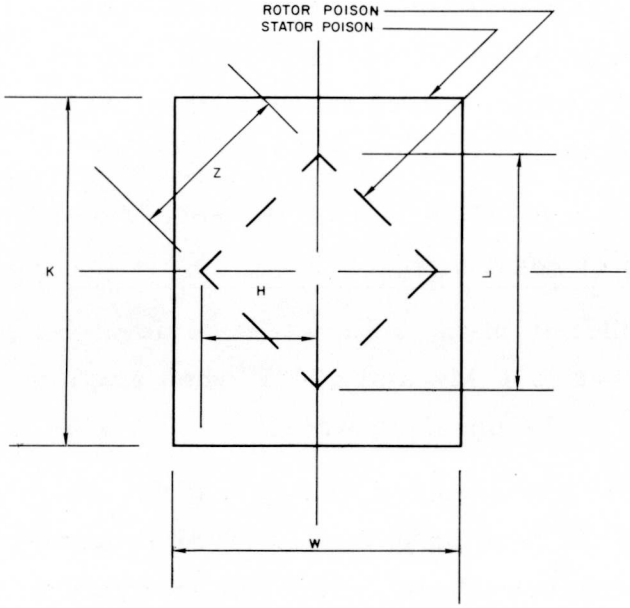

Figure 8. Relative Sizes of Rotor and Stator Squares

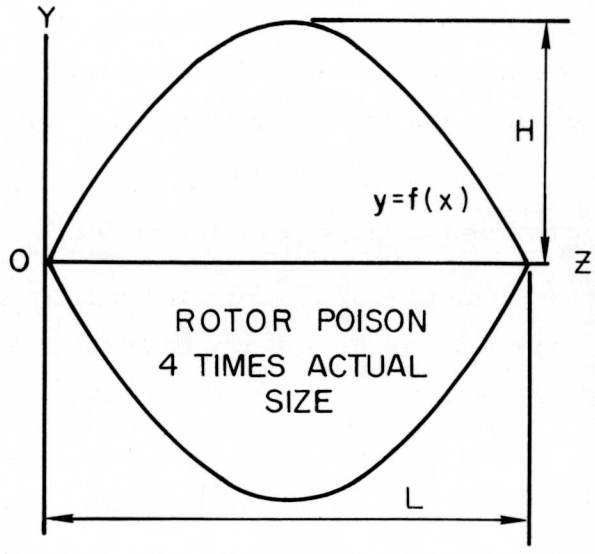

Figure 9. Theoretical Shape of Rotor Poison Square

set of poison squares. As seen in Table II, the variation is only too large at frequencies below about 0.005 cps.

The upper and lower bearings of the rotor operated at temperatures up to 500°F. They were made of graphite which was coated with Electrofilm to improve the wearing qualities when operating in a dry atmosphere of air or helium. The bearings were used only in an air atmosphere and performed satisfactorily.

The thimble and top shield plug were obtained from a Mark I control rod. The thimble was already equipped with grooves which were used to prevent the stator from turning in the thimble. The top shield plug was modified to adapt the existing control rod drive shaft to the oscillation drive shaft. A Torquestat was used to prevent damage to the mechanism if it jammed during operation.

Although no jamming occurred, the rotary device required a fairly large driving torque because of the O-ring seals on the drive shaft located in the top shield plug. The 3/4-hp motor on the drive mechanism was definitely needed when operating the device at 300 rpm (20 cps reactivity variation).

A protractor was added on top the shield plug for use in calibrating and determining the reactivity change vs angular position of rotary mechanism.

The unit was calibrated with the reactor critical at zero power. The automatic flux level controller was adjusted to peak sensitivity. A Veeder-Root counter which read to tenths of 1/16 in. was mounted directly on the control rod drive mechanism tower. Readings of control rod positions were taken as the rotary device was moved in 5 angular degree increments.

The resulting data is plotted in Figure 6 and indicates that the rotary unit provided a satisfactory sine wave variation of reactivity.

The use of aluminum facilitated construction of the rotary test device. However, it was necessary to limit reactor power to 1 Mw and 600°F when employing the aluminum device because of heating in the boral squares.

Zirconium construction had been planned for a second rotary test device. This would allow operation of the device at full reactor power and temperatures. Rare earth poisons would be employed to eliminate the (n, α) heating from boron-neutron absorption.

After initial tests with the aluminum rotary device, the next step was to investigate the possibility of sinusoidally operating a regular shim rod. This would allow data to be taken at any time without inserting a special reactivity device into the core. Due to successful operation of this method, it was unnecessary to fabricate the zirconium rotary device.

2. Scotch-Yoke Device

A Scotch-yoke device which would impart a sine wave motion to the ball-nut-screw mechanism of an SRE shim rod was designed and fabricated as shown in Figure 10.

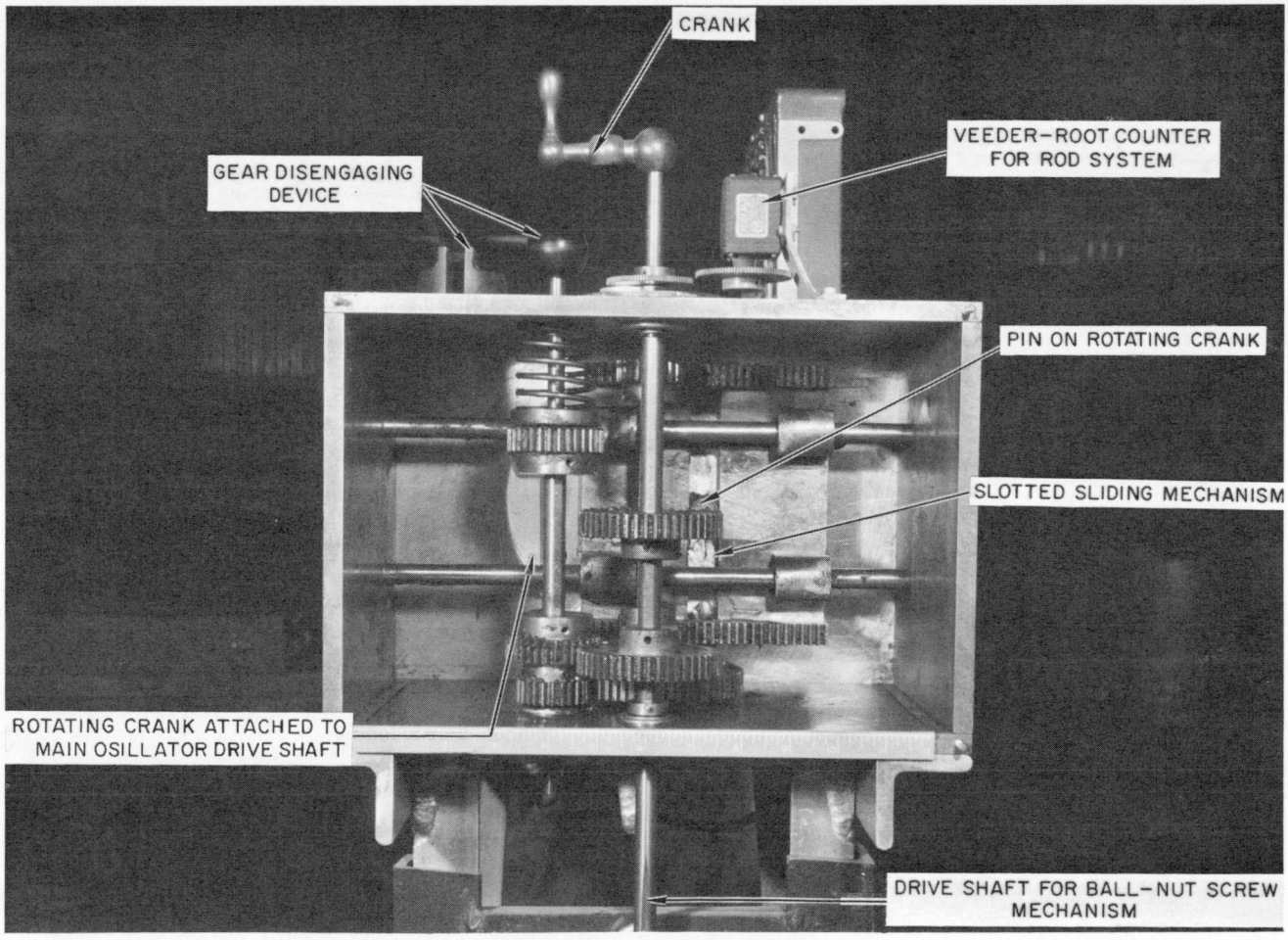

Figure 10. Scotch-Yoke Gear Box for Driving Control Rod Ball-Nut-Screw Mechanism With a Sinusoidal Motion

The Scotch-yoke mechanism is installed over the reactor face, and attached to the shim rod ball-nut-screw mechanism which is located below the face of the shield (Figure 11). This unit was successfully employed in obtaining all the "at power" frequency response measurements on the SRE.[4] A maximum frequency of 0.1 cps could be successfully obtained. Higher frequencies were possible but the large driving torque added additional phase shifts in the system.

The magnitude of the $\delta\rho$ variation could be varied by either: (1) changing the position of the pin on the face of the driving wheel — which determined the limits of motion of the sliding plate; or, (2) positioning the shim rod to operate at a different point on the differential rod worth curve.

The Scotch-yoke device with its associated gears, shafts, and bearings was designed to mount on the end of the drive unit as shown in Figure 11. The correlation equipment mounted on a servo plate, and geared to the same main drive shaft which attaches to the Scotch-yoke driving wheel can also be seen in Figure 11. Figure 11 also shows: (1) the protractor and its pointer (used for aligning the correlation equipment); (2) a universal joint; (3) a Torquestat to prevent damage to the equipment if the shim rod ball-nut-screw mechanism should jam; (4) a device for disengaging the drive gears to allow the shim rod to be moved manually to the desired location by turning the crank located on top of the Scotch-yoke mechanism box; and (5) a Veeder-Root counter to keep track of the shim rod location or distance it has been raised.

The only design difficulties encountered were those of suitable bearings for the mechanism. O-ring seals on the shaft of the shim rod mechanism are used to maintain a helium atmosphere in the shim rod thimbles. The seals impose a large friction load on the Scotch-yoke drive mechanism. This load caused the original bearings to fail. They were replaced with larger and higher quality bearings which were found to operate satisfactorily.

The coupling between the Scotch-yoke mechanism and the reactor face was the type with a ball bearing insert. It should be emphasized that couplings with any type of deformable rubber or plastic inserts should not be used in oscillator mechanisms as they will cause spurious phase shifts to be introduced into the measurements.

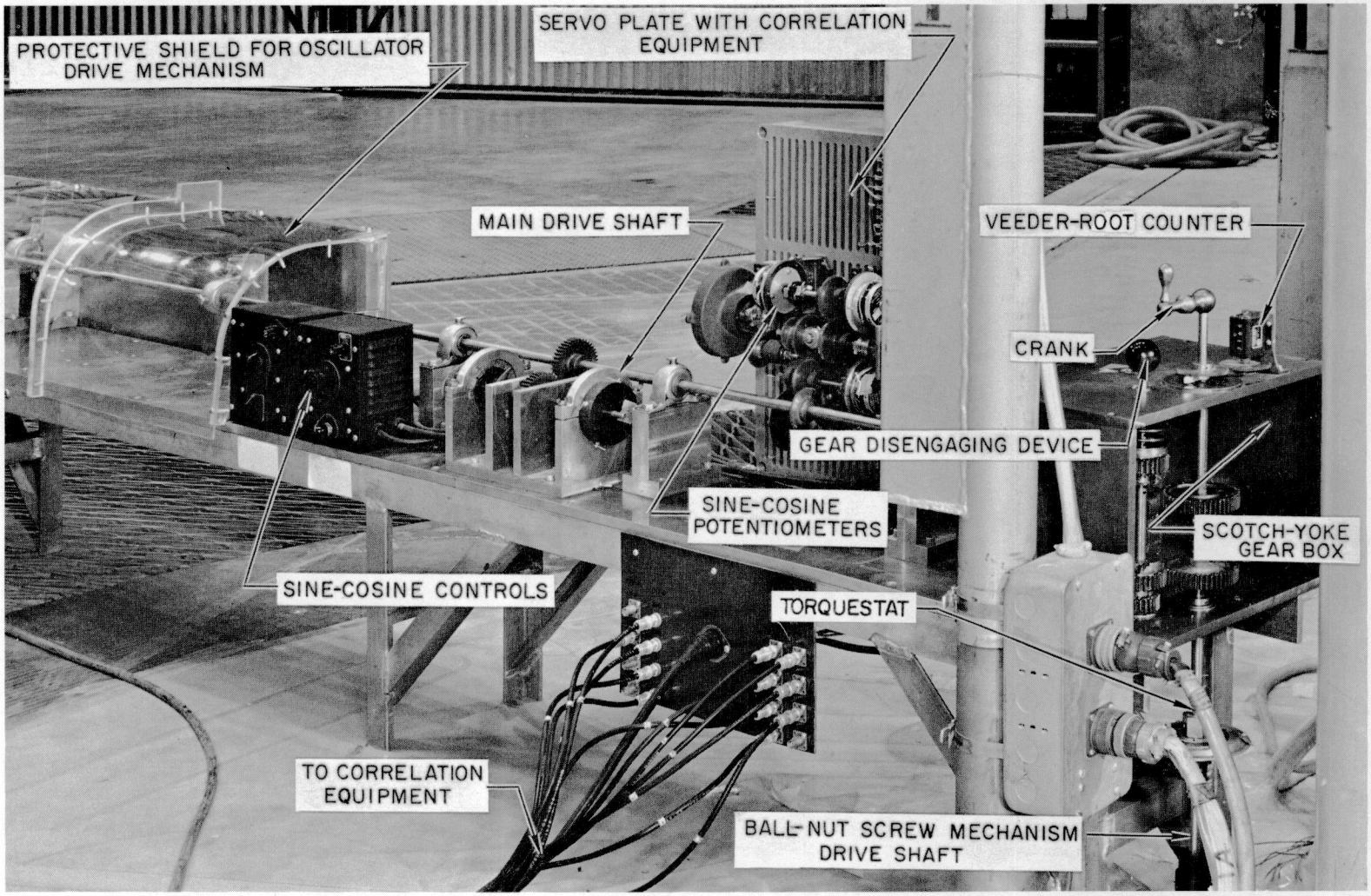

Figure 11. Scotch-Yoke Gear Box and Correlation Sine-Cosine Potentiometers in use With the Oscillator Drive Mechanism at the SRE

The Scotch-yoke mechanism was capable of sinusoidally oscillating a shim rod with a sine wave magnitude of 0.480 in., although in all the experiments the maximum shim rod motion was 0.256 in.

It would have been desirable if frequencies up to 1 cps could have been obtained with the Scotch-yoke device. This would have made it possible to obtain data at frequencies where both the "at power" magnitude and phase curves would match those for the zero power curves. This point deserves further elaboration and will be discussed later under experimental techniques, Section VI.

It can be stated that it was not possible to determine $\delta\rho$ with sufficient accuracy to directly determine the gain of the reactor at each frequency. Thus, to obtain the power coefficient, which is the difference between the reciprocals of the "at power" and zero power frequency response curves, it was necessary to match all curves at the high frequency end where the effect of the power coefficient approaches zero. This accounts for the need of obtaining data at frequencies considerably above the break frequency of the fuel time constant, which was the shortest time constant feedback effect in the SRE.

3. Direct Drive Device

A third means of sinusoidally varying reactivity was tested and found acceptable for obtaining amplitude data, but was not satisfactory for obtaining phase data. In this case, the shim rod was operated by the regular relay-servo drive system employed for automatic flux level control of the SRE. The L & N PAT automatic control unit was modified so that the feedback potentiometer on the shim rod drive - servo motor unit would be forced to follow a sine wave input signal to the PAT unit which contains a relay-servo loop. It must be noted that the rod drive - servo system had not been designed for high speed response, since this is not necessary for flux level control of the SRE. Nevertheless, it was possible to obtain good magnitude data at frequencies up to 0.05 cps, although the waveform appears quite jagged. If a continuous servo had been available, better results would have been obtained.

These tests were terminated when it became apparent that the Scotch-yoke mechanism was the most satisfactory for direct drive of the shim rod. The major difficulty with the direct drive device is that the transfer function of the relay servo must be considered in the data when employing the correlation technique

of measurement. The phase lag of this transfer function varies both with frequency and the magnitude of shim rod motion. The difficulty of having this additional transfer function will be evident when the correlation measurement technique is discussed.

C. MECHANICAL DRIVE MECHANISM

The mechanical drive mechanism was initially built to drive the rotary device, but was found to be satisfactory for the Scotch-yoke mechanism. It was also employed for driving a sine potentiometer to generate the sine wave input signal for the direct drive servo unit.

A 3/4 hp Servotek thyraton-controlled dc motor was chosen to drive the unit. It was equipped with tachometer feedback and capable of accurately holding any desired speed from 36 to 3600 rpm. This unit proved to be an excellent choice and greatly aided in obtaining selected oscillation frequencies.

A frequency range of 0.0002 to 20 cps, requires a shaft speed range of five decades, of which the motor speed control could give at best only two decades. Four additional decades of speed variation were obtained by the use of gear boxes. Three gear boxes with speed ratio of 10:1, 10:1, and 100:1 were employed. Figure 12 shows the motor and gear box units.

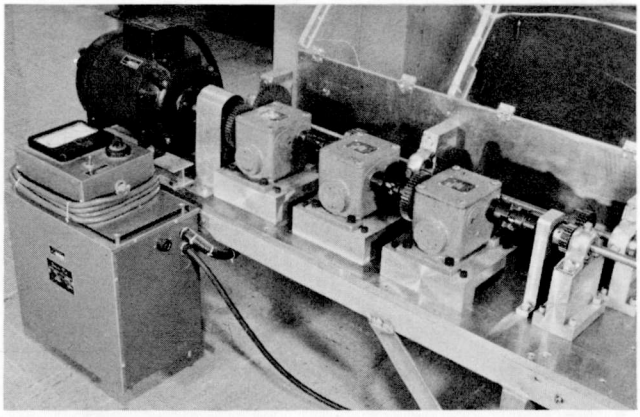

Figure 12. Special DC Motor Drive and Gear Boxes

Figure 13 shows the drive unit and Scotch-yoke mechanism installed. The servo plate with the correlation equipment may also be seen. A plastic shield was installed over the gear train as a safety feature. The length of the drive unit could have been decreased but at the time it was designed it was not known what additional gear boxes, etc., might be required.

The only design problems that were encountered were alignment and slippage of the gears on the shaft. Even though two heavy duty set-screws were used on each gear, it was found necessary to pin them to the shaft with removable, expanding pins in order to completely prevent slippage. Also, all couplings were of solid construction, with no rubber or deformable inserts.

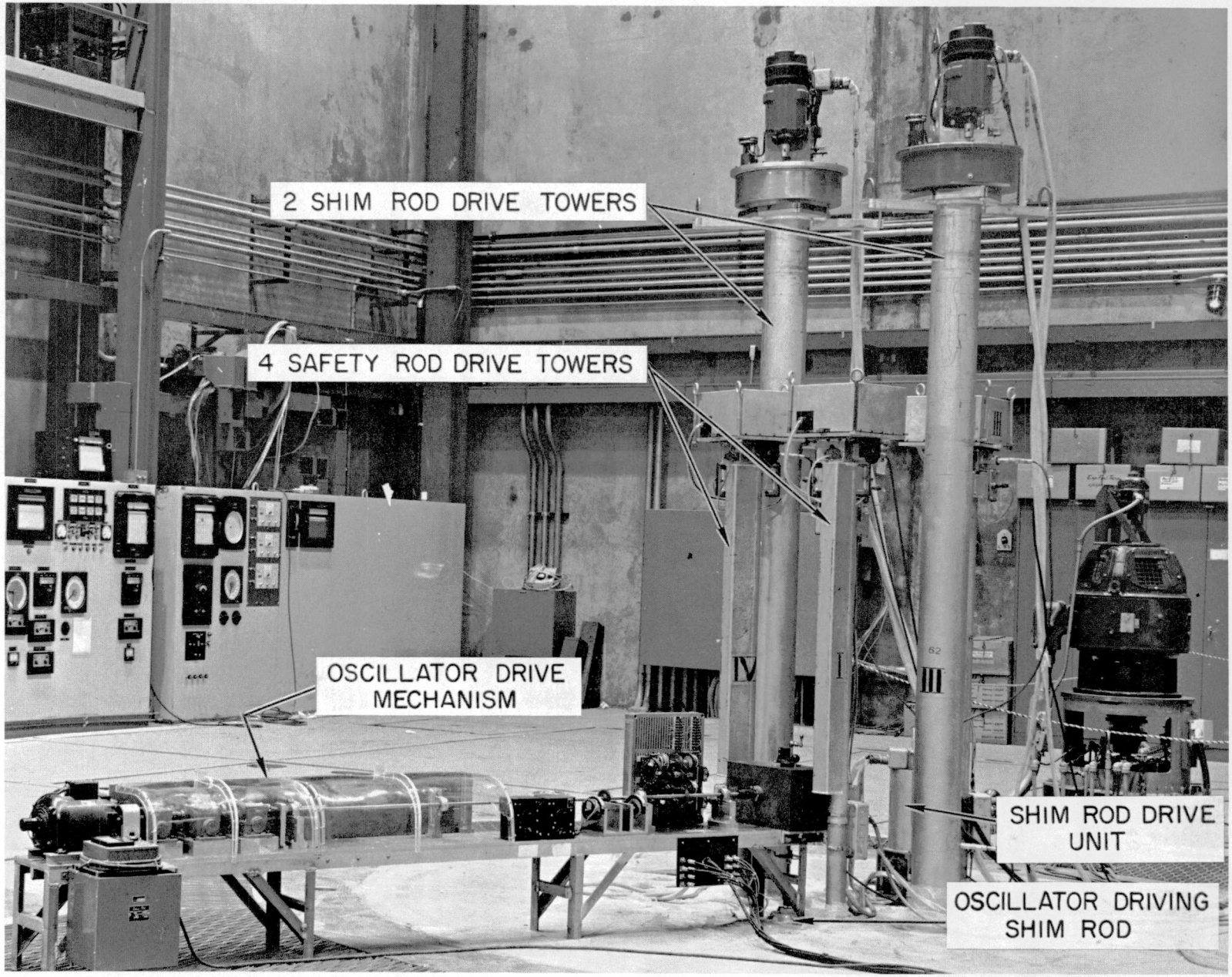

Figure 13. Entire Oscillator Mechanism in use During Oscillation Measurements at the SRE

V. MEASUREMENT OF REACTOR TRANSFER FUNCTIONS

A. REQUIREMENTS

At first it may seem a simple matter to record the power variation of a reactor along with an electrical representation of the reactivity variation, and directly measure the magnitude of the power variation, δn , and the phase difference between δn and the reactivity variation $\delta \rho$. In certain frequency ranges, this magnitude data may be accurate to a few percent, and the phase data accurate to ±5°. At high frequencies when $|\delta n/n|$ approaches 0.1%, noise distorts the power signal and directly recorded data become quite inaccurate. Fortunately a correlation type of measurement may be employed which makes it possible to obtain good data when the signal is equal to or even smaller than the noise level.

It is necessary to measure accurately $|\delta n|, |n_o|$, and the phase difference between δn and $\delta \rho$. For "at power" measurements, $|\delta T_f|, |\delta T_m|, |\delta T_c|$, and the phase differences between them and δn must also be measured, although the accuracy requirements are much less than those for $(\delta n/\delta \rho)(j\omega)$.

The measurements of $(\delta n/\delta \rho)(j\omega)$ at both zero power and "at power" represent the transfer or frequency response functions of the reactor. The difference between the reciprocal values of the "at power" and zero transfer functions is the true power coefficient of the reactor. Since this difference is small, good accuracy is necessary in the measurement of these two functions.

B. METHODS

During the course of the SRE transfer function measurements, three methods were used to measure the magnitude of reactor response, and the phase difference between this response and the reactivity forcing function. These were the (1) direct visual method, (2) quadrature components method, and (3) the null balance method. The null balance method is basically the same as the quadrature method.

Table IV shows the advantages and disadvantages of these methods. Each of the three methods will now be discussed.

TABLE IV

COMPARISON OF THE THREE METHODS FOR MEASURING REACTOR TRANSFER FUNCTION, GAIN, AND PHASE ANGLE

Method	Advantage	Disadvantage
Direct Visual Method	Fast, Direct	Difficult to obtain accurate phase data, especially if the noise level is high
Quadrature Components Method	Accurate phase and magnitude data even with small signal/ noise ratio	Needs 3 to 6 cycles of good data with no reactor power drift
Null Balance Method	Accurate phase and magnitude data even with small signal/ noise ratio. Eliminates computing phase and amplitude.	Time consuming to obtain null balance, that is, to align sine-cosine potentiometer wiper in phase with reactor response signal.

1. Direct Visual Method

Although Table IV indicates that this method is not as accurate, it was used at some extremely low frequencies, and for analyzing temperature data.

The data were recorded on Sanborn multichannel recorders of which ten channels were available.

The values of δn and $\delta \rho$ were normally recorded directly and side-by-side, as a means of checking the magnitude and phase data obtained by the correlation technique. For "at power" measurements, δT_f and δT_m were recorded along side δn, in order to obtain their respective phase shift from δn.

2. Quadrature Component Method

This method consists of determining both the magnitude of the component of δn that is in-phase with $\delta \rho$, and the magnitude of the component that is 90° out-of-phase with $\delta \rho$. δn is obtained from the square root of the sum of the squares of these two components. The tangent of the phase angle between δn and $\delta \rho$ is the ratio of the quadrature to the in-phase component of δn. This method of measuring these two components (discussed in detail in the Section IV-C-3)

has the characteristic that the noise part of the signal, as well as all harmonics in the signal, cancel to zero. Thus, it is possible to achieve an accurate measurement for δn magnitude and phase, even though the noise level is as large or larger than the signal level, and even though the reactor response signal contains harmonics from a slightly nonsinusoidal reactivity input.

3. Null-Balance Method

This is merely a special technique employed with the quadrature components method. The technique requires that the phase relationship of the wipers on a sine-cosine multiplying potentiometer be adjusted in such a manner during the measurement that the quadrature component goes to zero. In principal, this would allow a very accurate phase angle measurement.

C. INSTRUMENTATION

The instrumentation required to perform accurate transfer function measurements of a reactor will now be discussed. This will include the neutron detector, electrometer, and the correlation equipment required for the quadrature component method of measuring the magnitude and phase of δn with respect to $\delta \rho$. Figure 14 shows the instrumentation layout used during oscillation tests.

1. Neutron Detectors

For zero power transfer measurements only the reactor response must be measured. This was accomplished by employing Westinghouse boron-coated ionization chambers. These are the same chambers normally used for monitoring SRE reactor flux or power level.

2. Electrometer

The current from the ionization chamber was measured with a Keithley 410 electrometer. The electrometer was modified by removing the damping capacitors which are in the 10^{-8} ampere range. With these removed, the electrometer was satisfactory for use at frequencies up to 20 cps on the 10^{-8} ampere range. A 25-ft length of RG71 coaxial cable was used between the chamber and electrometer. Cable length was not critical in this case.

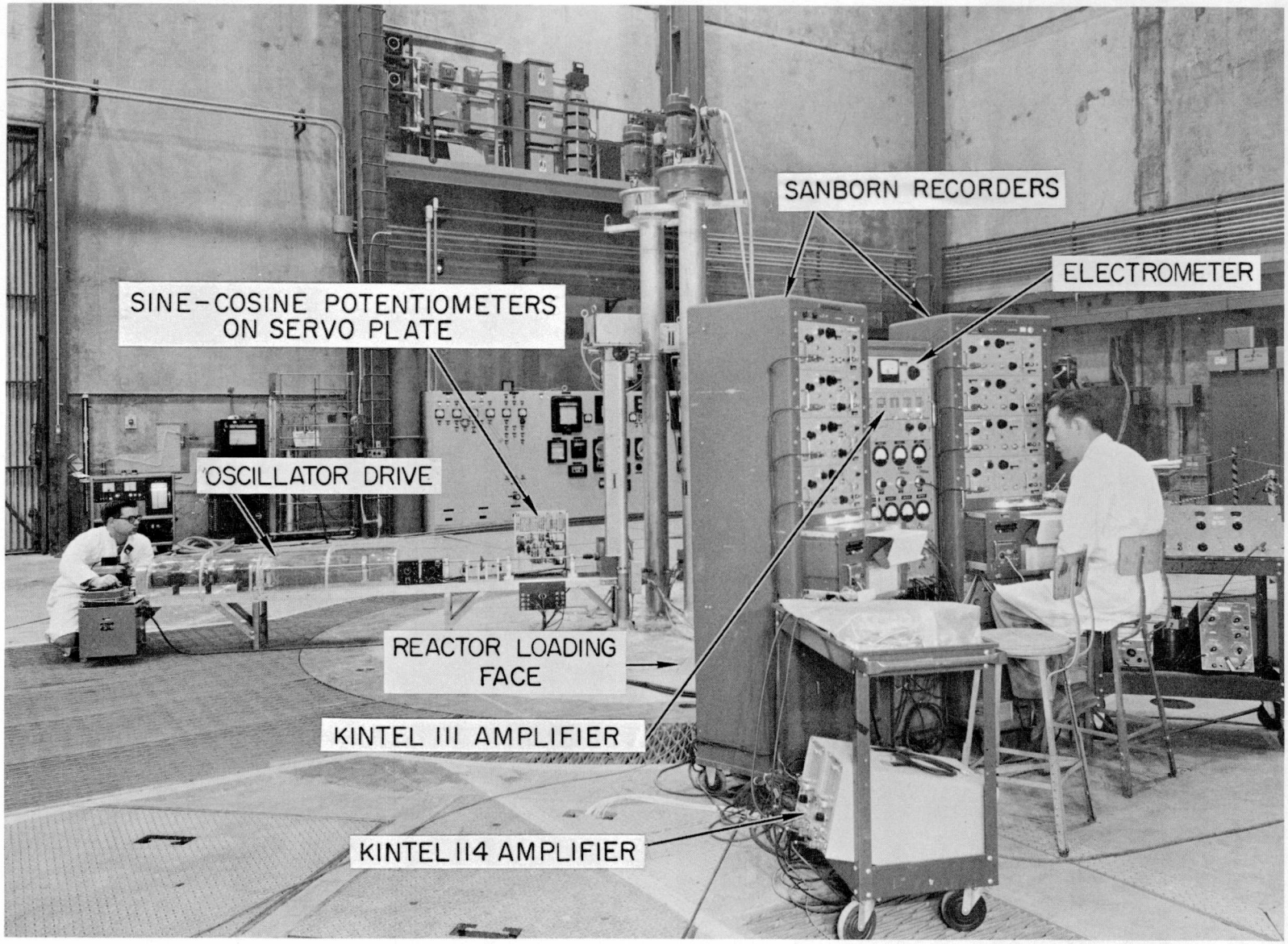

Figure 14. Oscillation Measurement Equipment Consisting of Recording Oscillographs, Operational Amplifiers, Electrometer, and Control Circuits

3. Correlation Equipment

Reference to Figure 15, and a brief explanation, will aid in understanding the design of the correlation equipment circuit. According to the theory developed in Appendix A, the reactor response $[\delta n \sin(\omega t+\theta)$ + harmonics + noise] must be multiplied by a signal representing $\delta\rho \sin\omega t$ and $\delta\rho \cos\omega t$. These products are then integrated to find the magnitude of the components of δn which are in-phase and in-quadrature with the reactivity input to the reactor, $\delta\rho \sin \omega t$.

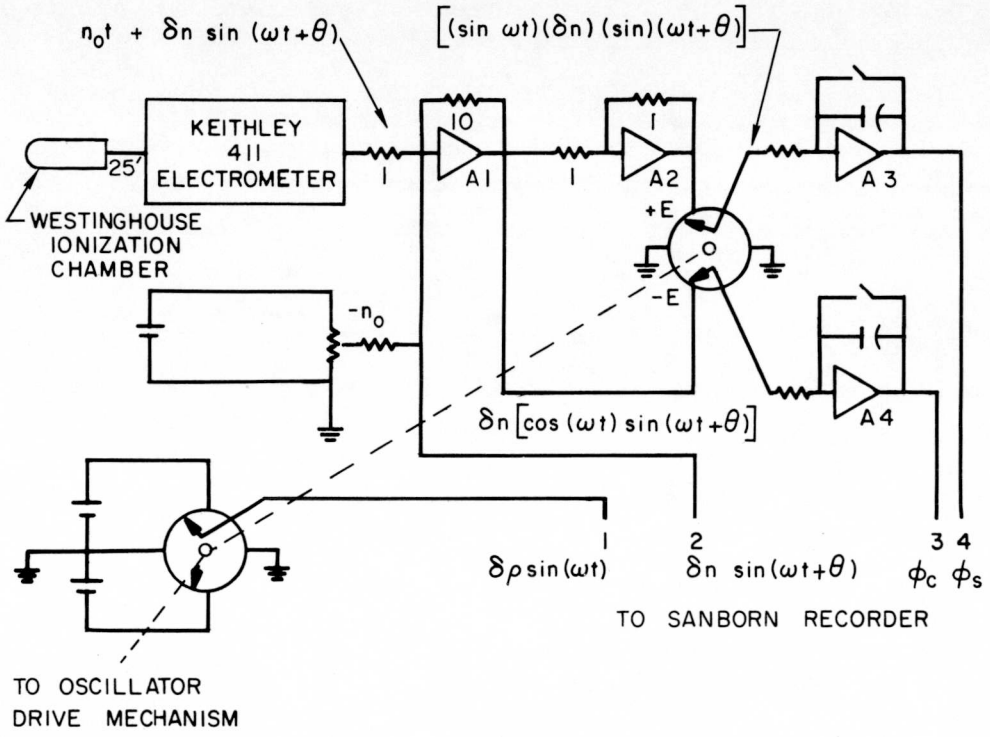

Figure 15. Circuit Layout for Correlation Measurement

The simplest method of performing the required multiplication is with a sine-cosine potentiometer. To obtain the proper voltages across the sine-cosine potentiometer, it is necessary to use an inverting operational amplifier with a 1:1 resistor network. It is also necessary to bias out the n_o value, both to prevent overloading the operational amplifier, and damaging the sine-cosine potentiometer.

The voltage across the potentiometer represents $[\delta n \sin(\omega t+\theta)$ + harmonics + noise]. The positions of the wipers are equivalent to $\delta\rho \sin \omega t$ and $\delta\rho \cos \omega t$, and will give the following two products:

1) $\delta\rho \sin \omega t[\delta n \sin (\omega t+\theta) + \text{harmonics} + \text{noise}]$

2) $\delta\rho \cos \omega t[\delta n \sin (\omega t+\theta) + \text{harmonics} + \text{noise}]$

To obtain the time integral of the above two products, the output of the wipers of the sine-cosine potentiometers are fed to Kintel Type 111 operational amplifiers, used as integrators. The outputs of these two integrators are recorded on Sanborn recorders. Typical Sanborn chart records are shown in Figures 16 and 17. The slopes of the recordings are the quantities needed to calculate $|\delta n|$ and its phase angle.

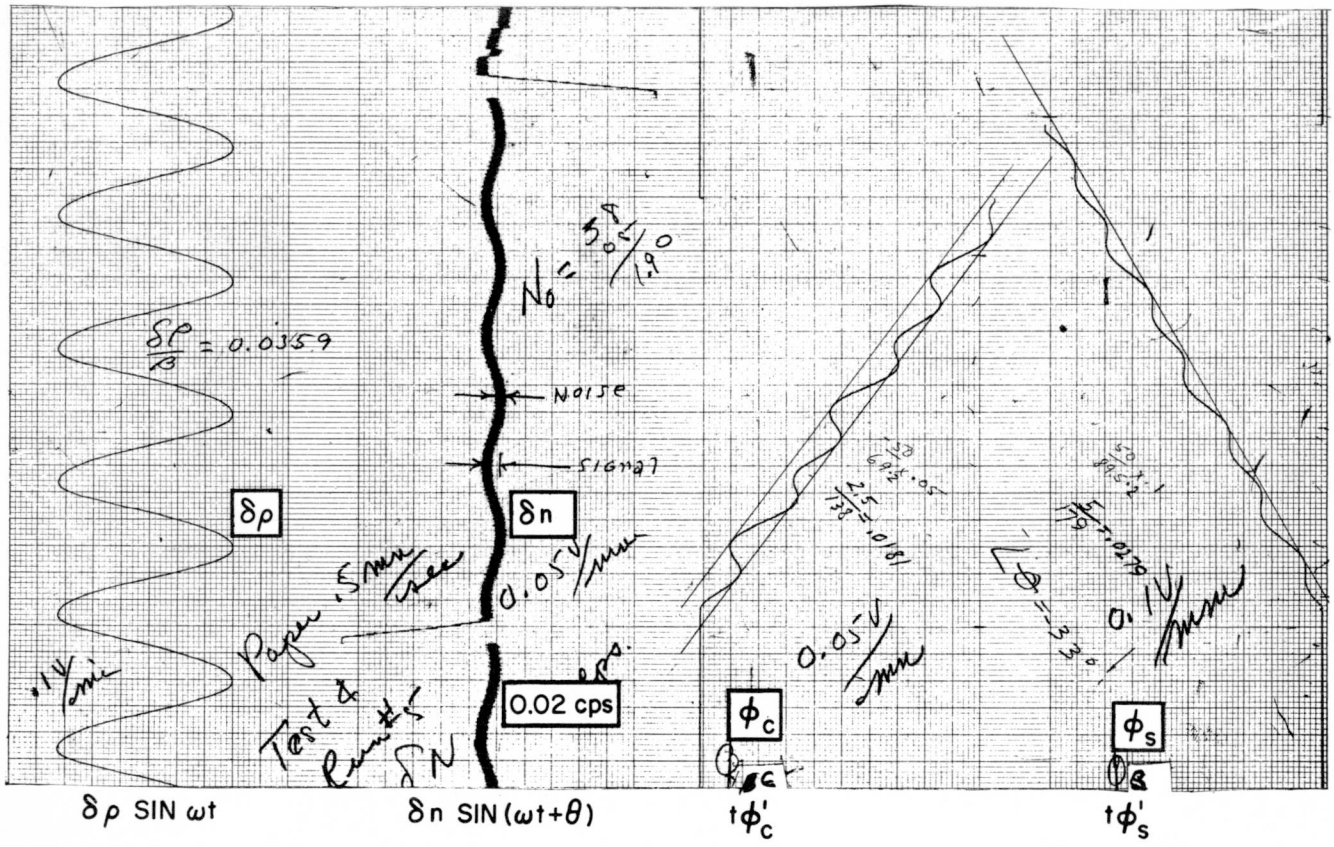

Figure 16. Typical Oscillograph Record of Reactor Tests Employing Scotch-Yoke Reactivity Device

When the recorder pen reaches full scale, the condenser in the integrating amplifier is manually discharged and the process repeated. This technique has been used to overcome the problem of obtaining a long time constant RC network in the integrating amplifier. Other investigators have used Velodyne

integrators which can have a long time constant. For the SRE measurements, the technique of discharging the integrating condenser was entirely satisfactory.

4. Sine-Cosine Potentiometers

The selection of suitable sine-cosine potentiometers was one of the more troublesome parts of the experiment. The original potentiometers were wire-wound 20,000 ohm units. This is the resistance of either (1) one quadrant, or (2) the total resistance between the +E and -E terminals. The high resistance required a very small wire size and the units soon failed, even before being operated at the maximum required speed of 20 cps or 1200 rpm.

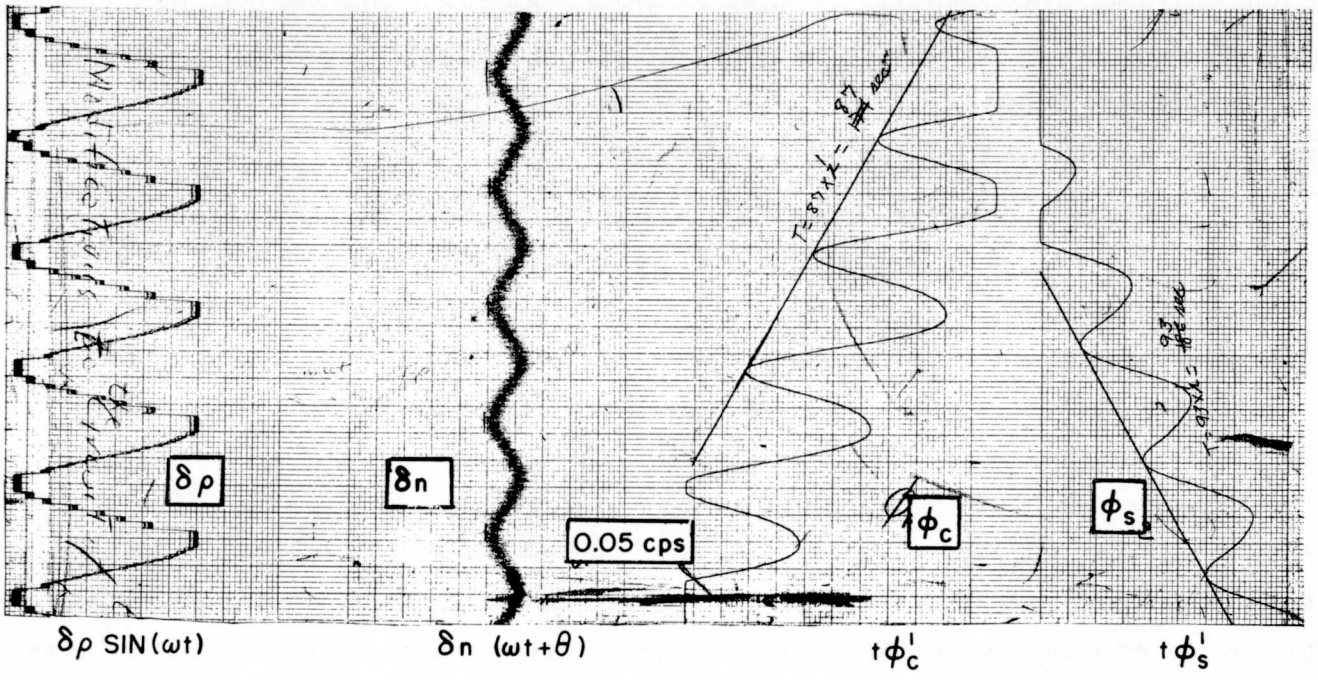

Figure 17. Typical Oscillograph Record of Reactor Tests Employing Direct Drive Reactivity Device

The next sine-cosine potentiometers selected were the carbon-deposited type, 5,000 ohm per quadrant, ball bearing equipped, Model 206 with a linearity of 0.25%. They were manufactured by Computer Instruments Corporation and they have proven to be a good choice.

In order to achieve the maximum possible linearity when using these sine-cosine potentiometers, it is necessary to specify the external resistance connected to the wipers, when ordering. In this case, these are the input resistances of the two operational amplifiers employed as integrators.

5. Servo Plate Details

The sine-cosine potentiometers were initially geared directly to the main horizontal drive shaft of the mechanical drive unit. Due to the difficulty of accurately aligning the zero position of the sine wiper with the zero position of reactivity variation of either the rotary or the Scotch-yoke reactivity mechanism, it was decided to couple the potentiometers to the main drive shaft via a mechanical differential. At this point, the desirability of mounting all this equipment on a servo plate became evident. Figure 18 shows the servo plate with two sine-cosine potentiometers, differentials, alignment drive motors, and phase-measuring direct-reading angle scales. Two potentiometers that are directly geared to the main drive shaft can also be seen in Figure 18.

Close inspection of Figure 18 will show that although the phase of sine-cosine potentiometer 3 may be changed by the adjusting motor 3, this will also change the phase of sine-cosine potentiometer 4. This particular feature was installed for use with the direct drive method of achieving sinusoidal reactivity variations. The object was to first perform a null-balance type of correlation measurement, between the electrical sine wave input signal to the modified PAT relay servo unit, and the resultant shim rod motion. This had the effect of correctly positioning the sine wipers on sine-cosine potentiometer 4 to match the shim rod motion and the sinusoidal reactivity input to the reactor. Although the technique was used in a few tests, the direct drive method was found to be less satisfactory for frequency response measurements than either the rotary or Scotch-yoke mechanisms, and effort was discontinued on this device. Being a sufficiently novel method of directly and accurately eliminating the phase shift of an intermediate transfer function in frequency response measurements, the technique may prove valuable in oscillation experiments on other types of reactors.

When employing the null-balance method, attempts were made to read the phase angle directly from angle scales mounted on the servo plate. It was found that this was possible only if the backlash in the gear trains was removed by

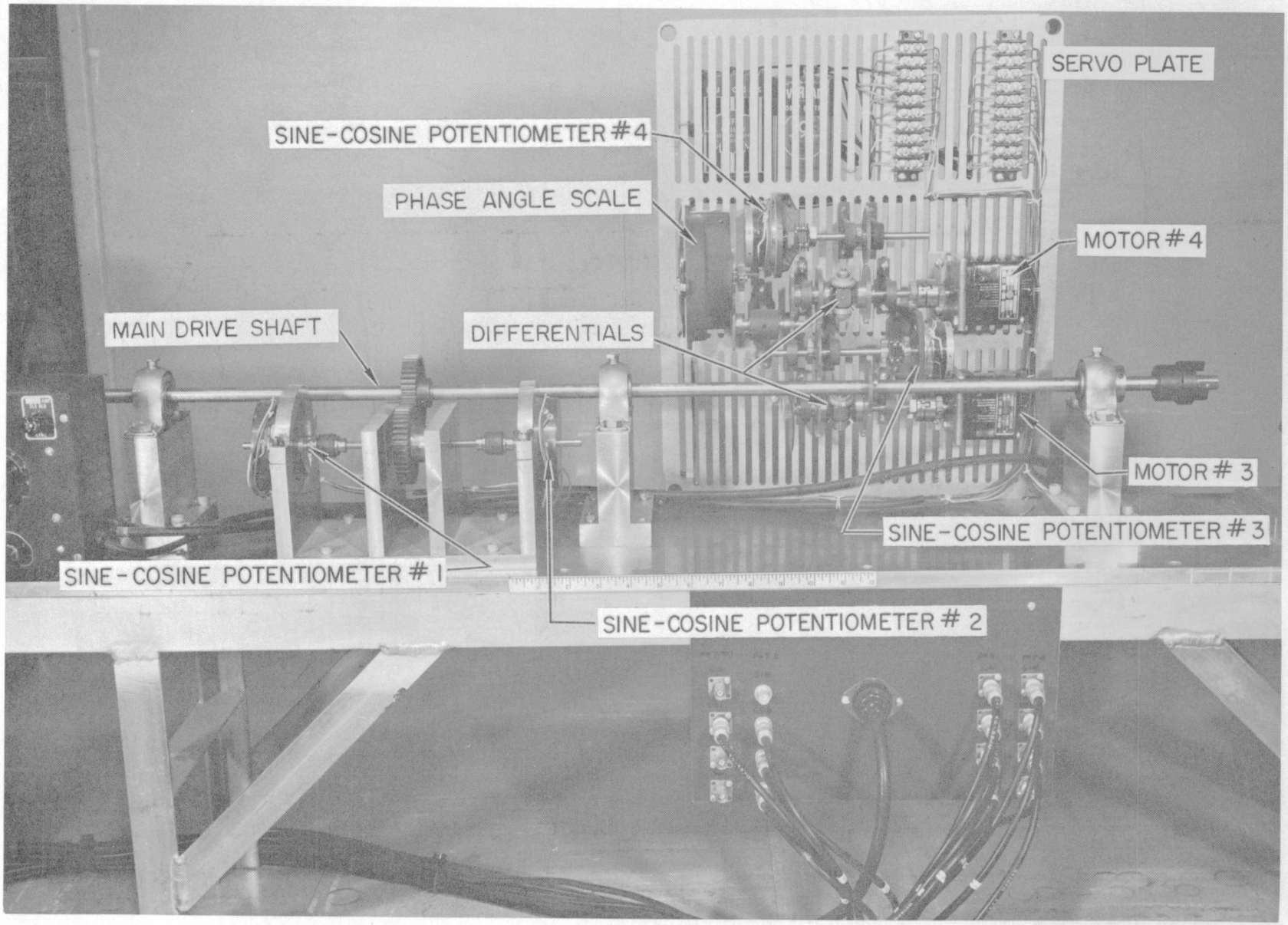

Figure 18. Servoplate Containing Sine-Cosine Potentiometers and Phase Adjusting Differentials Employed for Correlation Measurements

approaching the null-balance point from the same direction, and with no overshoot. Although high quality gears and differentials were employed, the backlash added up to a few mechanical degrees.

For this reason, the sine-cosine potentiometers were initially aligned with the reactivity device and left in this position. Phase angles were usually obtained by the quadrature components method. Although the null-balance method was time consuming at low frequency measurements, the backlash problem was another reason for not using it.

The servo plate components have operated satisfactorily at speeds up to 1200 rpm for obtaining 20 cps frequency response data.

D. SPECIAL EQUIPMENT FOR "AT POWER" MEASUREMENTS

For the "at power" measurement, it is necessary to measure the magnitude and phase relationship of selected fuel and moderator temperatures with reference to the reactor response, δn. These temperatures were measured with permanently installed thermocouples. Since the variables of interest are small temperature changes, δT_f and δT_m, thermocouples are entirely adequate for these measurements. Figure 19 is a schematic of the circuit employed. Most of the thermocouple signal was biased out with a dc potential before being inserted into the Kintel 114, full-floating, true differential amplifier. The amplified signals were then either directly recorded or employed for correlation measurements.

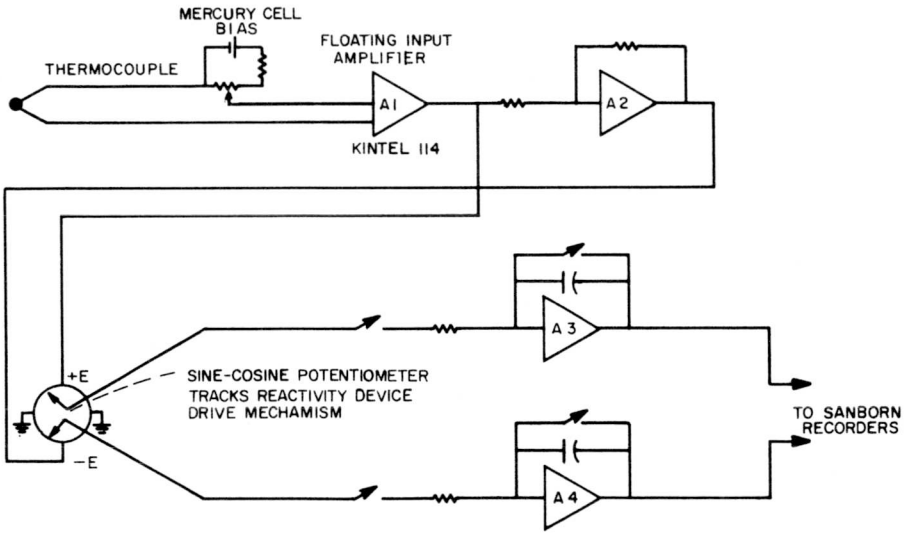

Figure 19. Circuit Layout for Oscillation Temperature Measurement With Correlation Method

VI. EXPERIMENTAL TECHNIQUES AND ANALYSIS OF DATA

A. INTRODUCTION

The major reason for the zero power, reactor frequency response function measurements was to determine the validity of the experimental techniques to be employed in the program of oscillator experiments on the SRE.

Although the rotary reactivity device was employed for the zero power tests, the Scotch-yoke mechanism was found to give equally good results up to a frequency of .05 to 0.1 cps, and, as such, was employed for all the "at power" measurements. The direct drive method produced poor phase data but the amplitude response data was correct. The direct drive method was therefore found convenient for calibrating SRE shim rods by oscillation techniques. This technique gave excellent results which checked within 6% of the rod-bump-period method results of shim rod calibration. The oscillation method of rod calibration takes only about one-sixth the time required by the rod-bump-period method — once the equipment is set up. The saving of time results from the fact that the average power level of the reactor is not changed, and no time is required for the delayed neutron population to return to equilibrium — as is the case in rod bump-period tests. A full discussion of the oscillation technique for shim rod calibration is given in Reference.[2]

The details of the experiments utilizing the rotary device will now be discussed.

B. MEASUREMENTS UTILIZING ROTARY DEVICE AND CORRELATION EQUIPMENT

After installing the rotary device and thimble in the core, the first problem was to determine its waveform and magnitude of reactivity variation. A plot of the waveform would also indicate the best choice for the zero reactivity position. With the rotor in its zero reactivity position, the sine wiper on the sine-cosine potentiometer was aligned at its zero position. This was done by either (1) the aid of a Kintel Model 425A microvoltmeter connected between the wiper terminal and the ground connection, with a voltage on the +E and -E terminals, and with the wiper alignment set to produce a null reading; or (2) the wiper output was

integrated on the appropriate integrating amplifier and its alignment set to produce a zero time rate-of-change in the integrator output.

The proper gear box ratios were then set and the required motor speed calculated. The motor was brought to the proper speed with its speed control. At this time, the reactor power was oscillating an amount determined by the frequency of oscillation – since the amount of reactivity variation of the rotary device is constant. With the Scotch-yoke mechanism, the amount of reactivity variation could be adjusted as mentioned previously.

The next procedure concerned making certain that the average power level of the reactor was stable. If it was drifting, a small reactivity correction was made with a shim rod. Quite often the correction consisted of such a short "on time" for the shim rod drive motor that it was difficult to perform without an overcorrection. Attempts were made to allow for this correction by initially setting the oscillator rotor at a position where the reactor would be subcritical if the rotor was returned to its zero reactivity position, and the position of the shim rods was not changed. The method did not completely solve the drift problem, probably because the reactor was not always exactly critical at the start of the oscillation measurement. For this reason, it was invariably necessary to readjust a shim rod to obtain a constant average reactor power level during reactor oscillation.

The next step was to measure the magnitude of the reactor power variation, δn, and the phase angle between δn and $\delta \rho$. The reactor power level, n_o, was also to be measured. Actually, the only magnitude measurement needed is the ratio $|\delta n/n_o|$.

A direct visual measurement was always made by recording δn, and a signal generated by a sine-cosine potentiometer which represented the reactivity variation, $\delta \rho$. These were recorded side-by-side on a four channel Sanborn recorder. A typical chart record is shown in Figure 20. This allowed a determination of $|\delta n|$ and the phase angle, θ. The value of n_o was determined by either measuring the value of the bucking voltage or the average output voltage of the electrometer.

A correlation measurement was also performed, and it was by this method that the most accurate phase data was obtained. Figures 16, 17, and 20 also show the recorded correlation data. At least three to five complete cycles of

oscillation with no reactor power level drift are necessary to obtain an accurate measurement. The slopes of the recorded data are the numbers needed for determining δn and θ. That is,

$$\delta n = 2\sqrt{\phi_s'^2 + \phi_c'^2} \qquad \theta = \tan^{-1}\frac{\phi_c'}{\phi_s'}$$

The signs of ϕ_s' and ϕ_c' must be considered in order to ascertain the correct quadrant for the angle, θ.

The effect of the integration process on a second harmonic term, which occurs when integrating the product of two sine-cosine terms, can be easily seen in Figure 16. As shown in Appendix A, this effect always integrates to zero over a complete cycle.

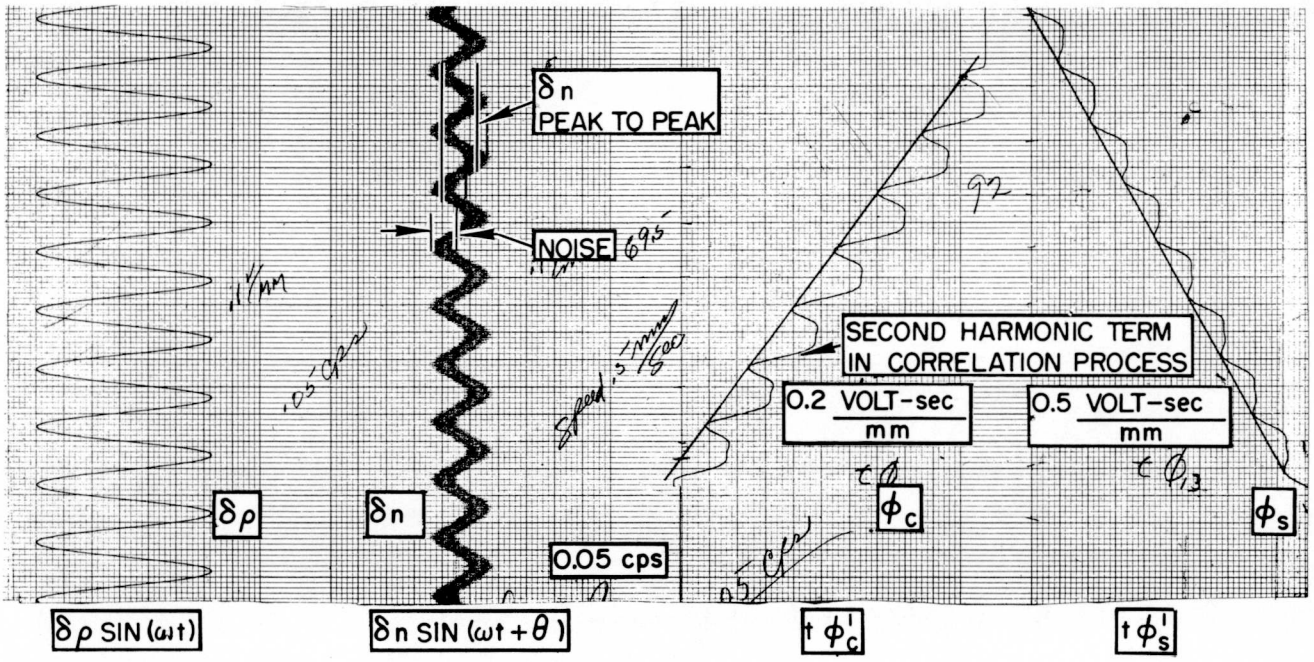

Figure 20. Typical Oscillograph Record of Reactor Tests Employing Rotary Device

C. ANALYSIS OF DATA

The details of the method of analyzing the data recorded in Figure 20 will now be discussed.

Referring to Figure 20, the first column on the left is an electrical representation of the reactivity variation $\delta\rho$, and is an electrical signal from a sine potentiometer. In column two, the reactor power response, δn, is recorded directly, and includes noise and harmonics in addition to the fundamental frequency of reactor response. The amplitude of $|\delta n|$ affords a check on the $|\delta n|$ calculation obtained utilizing ϕ_s' and ϕ_c', in the quadrature components method. A comparison of the phase lag between column one and two assists in eliminating quadrant errors on the phase angle, θ.

Calculations made from data obtained from the 3rd and 4th columns of Figure 20 are as follows: (See Appendix A for the derivation of the equations)

f = 0.05 cps, chart speed 0.5 mm/sec, integration time constant, 1 second

$$\phi_c' = \frac{\phi c}{t}$$

$$\phi_c' = \frac{0.2 \frac{\text{volt sec}}{\text{mm}} \times 50\,\text{mm}}{\frac{69.5\,\text{mm}}{0.5\,\text{mm/sec}}} = 7.2 \times 10^{-2}\ \text{volts}$$

$$\phi_s' = \frac{\phi s}{t}$$

$$\phi_s' = \frac{0.5 \times 50 \times 0.5}{92} = 13.6 \times 10^{-2}$$

$$\delta n = 4\sqrt{\phi_c'^2 + \phi_s'^2} = \text{peak-to-peak value}$$

$$\delta n = 4(10)^{-2}\sqrt{(7.2)^2 + (13.6)^2} = 0.595\ \text{volts peak-to-peak}$$

$$\theta = \tan^{-1}\frac{\phi_c'}{\phi_s'}$$

$$\theta = \tan^{-1} \frac{7.2}{13.6} = 28° \text{ phase lag}$$

n_o = 18.8 volts (measurement not shown)

$$\frac{\delta\rho}{\beta} = 0.023 \text{ (rotor peak-to-peak reactivity worth)}$$

$$G(j2\pi f) = \left| \frac{\delta n}{n_o} \frac{\beta}{\delta\rho} \right| \angle\theta$$

$$G(j2\pi 0.05) = \left| \frac{0.595}{18.8} \times \frac{1}{0.023} \right| \angle -28° = 1.38 \angle -28° = 2.8 \text{ db} \angle -28°$$

The result is seen to agree with the theoretical value as shown in Figure 21.

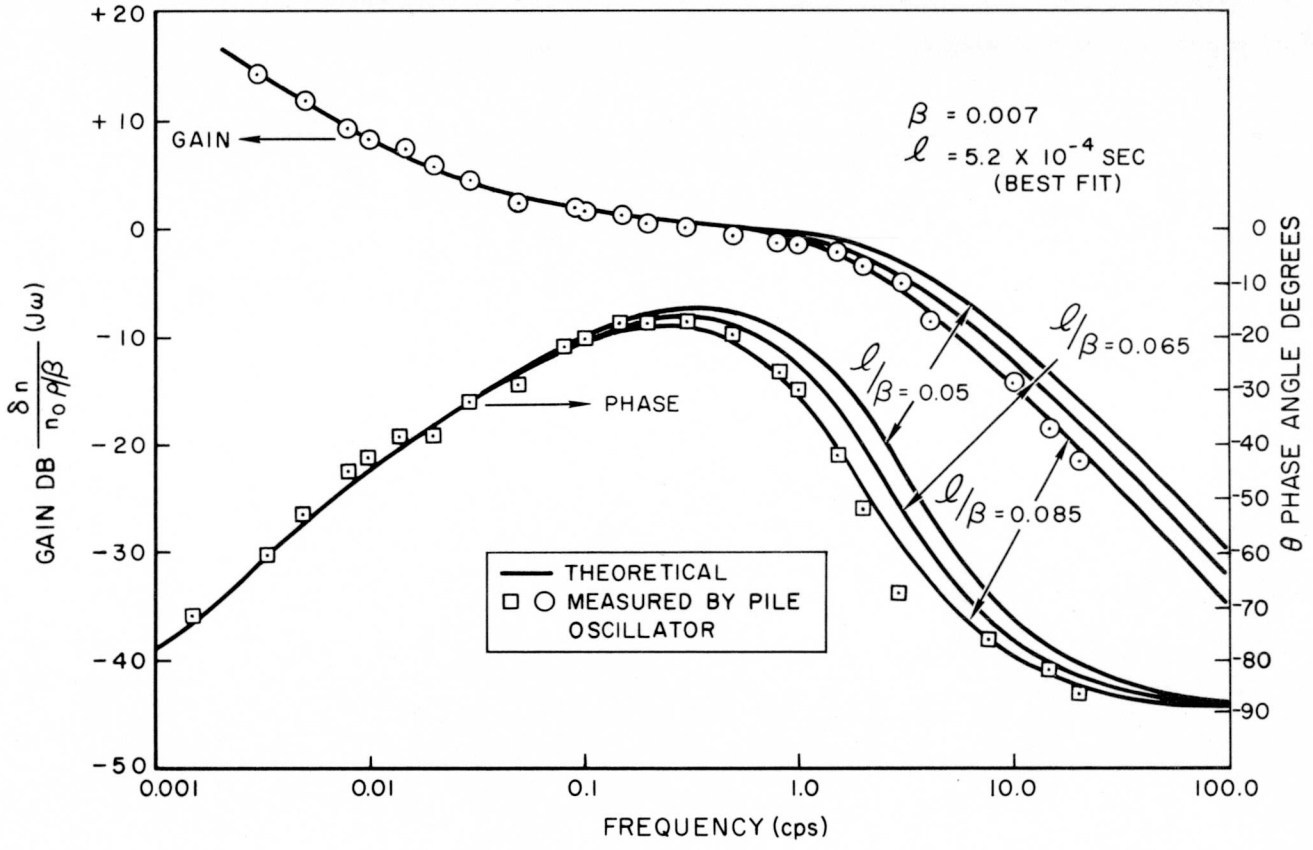

Figure 21. SRE Zero Power Transfer Function

VII. INTERPRETATION OF EXPERIMENTAL RESULTS

Figure 21 shows the results of the reactor zero power frequency response function measurements on the SRE at frequencies from 0.005 to 20 cps. Also plotted in Figure 21 are three theoretical curves for the reactor zero power frequency response. It can be seen that the measured data best fit the theoretical curve for an ℓ/β value of 0.075 sec. If the value of β for the SRE is chosen as 0.007, the value for the prompt neutron lifetime in the SRE is $(5.25 \pm 0.35) \times 10^{-4}$ seconds. This compares favorably with the theoretical calculated value of 5.0×10^{-4} seconds and with the value of $(5.25 \pm 0.70) \times 10^{-4}$ seconds obtained by random noise experiments on the SRE.[5]

The close agreement between the experimental data and the theoretical reactor frequency response curves indicates that; (1) the small signal theory is satisfactory, and (2) that the experimental techniques employed for the measurements are satisfactory.

VIII. SUMMARY AND CONCLUSIONS

The program to measure the zero power and "at power" frequency response functions of the SRE required the development and testing of equipment for varying the reactivity and measuring the amplitude and phase angles of sinusoidal signals. The amplitudes of those signals were in many cases, comparable to the signal noise level.

The program for zero power reactor transfer function measurement led to the useful development of both a rotary and a Scotch-yoke mechanism that produced sinusoidal variations in reactivity. A third method, the direct drive method, while not suitable for transfer function measurements was useful for control rod calibrations utilizing oscillation techniques.

Also, the correlation method of measurement was developed to produce accurate amplitude and phase angle measurements, as required for this program.

The zero power frequency response function measurement on the SRE confirmed the experimental methods employed. The experimental data correlated quite well with the linearized zero power reactor transfer function, and the measurements provided an experimentally determined value of ℓ/β for the SRE.

APPENDIX: DEVELOPMENT OF CORRELATION MEASUREMENT THEORY AND METHOD

The use of a correlation measurement technique has become a common experimental technique where sinusoidal signals are involved – especially where the signal-to-noise ratio is low.[6]

The technique, as introduced in Section V-C-3 of this report, is a method for obtaining the in-phase and quadrature components of the desired variable, in relation to the sinusoidal forcing function. The correlation technique allows an accurate measurement of these two components even though the signal-to-noise ratio is much less than unity, due to the presence of harmonics or random noise in the signal.

The technique involves multiplying the signal which represents the response of the system by: (1) a signal which represents the input to the system, and (2) a signal with a 90° phase difference. Since the input signal for this method is proportional to $\sin \omega t$, the other signal is proportional to $\cos \omega t$. The two products are then integrated with respect to time. When the integration is over a complete cycle of the input signal, the derivations will show that the integration process results in all terms having a zero value, except the desired terms. Thus, the effects of harmonics and noise result in a null, and the value of the desired response signal may be extracted from a signal with large noise level.

The input signal to the reactor may be represented as

$$\delta\rho = \delta\rho \quad \sin \omega t.$$

The response of the reactor, including harmonic terms and noise will be as follows:

$$\delta n = \delta n \quad \sin(\omega t + \theta) + \text{Harmonics} + \text{Noise}.$$

The two products required are as follows:

$$P_1 = \left[\delta n \quad \sin(\omega t+\theta) + H + N\right] \sin \omega t,$$

and

$$P_2 = \left[\delta n \quad \sin(\omega t+\theta) + H + N\right] \cos \omega t.$$

In the integrals required, ω has been replaced by $2\pi/T$, and T is the period of oscillation as follows:

$$\phi_s = \int_o^{cT} \left[\delta n \quad \sin\left(\frac{2\pi t}{T} + \theta\right) + H + N\right] \sin \frac{2\pi t}{T} dt \quad ,$$

and

$$\phi_c = \int_o^{cT} \left[\delta n \quad \sin\left(\frac{2\pi t}{T} + \theta\right) + H + N\right] \cos \frac{2\pi t}{T} dt \quad ;$$

where c is the number of complete cycles of oscillation over which the integral is taken.

Disregarding the harmonic and noise terms for the moment, the results of the two integrals are as follows:

$$\phi_s = \delta n \quad \frac{cT}{2} \cos\theta \quad ,$$

and

$$\phi_c = \delta n \quad \frac{cT}{2} \sin\theta \quad .$$

It is desirable to express cT in terms of the total time elapsed, t, as follows:

$$\phi_s = \delta n \ \frac{t}{2} \cos\theta \quad ,$$

and

$$\phi_c = \delta n \ \frac{t}{2} \sin\theta \quad .$$

Rearranging,

$$\frac{\phi_s}{t} = \delta n \ \frac{\cos\theta}{2} = \phi_s' \text{(slope)} \quad ,$$

and

$$\frac{\phi_c}{t} = \delta n \ \frac{\sin\theta}{2} = \phi_c' \text{(slope)} \quad ,$$

where $\phi_s' = \phi_s/t$ and $\phi_c' = \phi_c/t$ are the slopes of the integration data as shown in Figures 16, 17, and 20.

The next step is to take the square root of the sum of the squares of the two above equations, obtaining

$$\sqrt{\phi_s'^2 + \phi_c'^2} = \frac{\delta n}{2} \sqrt{\text{Cos}^2\theta + \sin^2\theta} = \frac{\delta n}{2} \quad ,$$

or

$$|\delta n| = 2\sqrt{\phi_s'^2 + \phi_c'^2} \quad .^*$$

*Note: In the numerical example, calculation of both δn_o and $\delta\rho$ are taken as peak-to-peak values for convenience of measurement.

The ratio of the two equations gives

$$\frac{\phi_c'}{\phi_s'} = \frac{\sin\theta}{\cos\theta} = \tan\theta \quad ,$$

or θ, the phase angle:

$$\theta = \tan^{-1}\frac{\phi_c'}{\phi_s'} \quad .$$

All harmonic and noise effects may be expressed as a sum of sine and cosine terms of different magnitudes and frequencies such as:

$$\text{Harmonics + noise terms} = \sum_{n=2}^{\infty} A_n \sin n\omega t + \beta_n \cos n\omega t$$

δn is given by

$$|\delta n|_{\text{peak-to-peak}} = 4\sqrt{\phi_s'^2 + \phi_c'^2} \quad .$$

The following two integrals must now be considered:

$$\phi_s = \int \sin\omega t \sum_{n=2}^{\infty} \left(A_n \sin n\omega t + \beta_n \cos n\omega t\right) dt \quad ,$$

and

$$\phi_c = \int \cos \omega t \sum_{n=2}^{\infty} \left(A_n \sin n\omega t + \beta_n \cos n\omega t \right) dt \quad .$$

It can be shown that the following four integrals are always equal to zero, when integrated over any number of complete cycles of the fundamental frequency ω:

$$\int_o^{cT} \sin \omega t \sin n\omega t \, dt = 0 \quad ,$$

$$\int_o^{cT} \sin \omega t \cos n\omega t \, dt = 0 \quad ,$$

$$\int_o^{cT} \cos \omega t \sin n\omega t \, dt = 0 \quad ,$$

$$\int_o^{cT} \cos \omega t \cos n\omega t \, dt = 0 \quad ;$$

where c is the number of complete periods, T over which the integral is evaluated.

There is one more item that needs to be considered and that is the effect of a drift in average reactor power. This would introduce a term of a form $bn_o t$, where b is a constant.

The integrals and results to consider are as follows:

$$\phi_s = \int_o^{cT} bn_o t \sin \omega t \, dt = - \frac{bn_o cT}{\omega}$$

and

$$\phi_c = \int_o^{cT} bn_o t \cos \omega t \, dt = 0 \quad .$$

It can thus be seen that the effect of a drift in reactor power will be to add another term to ϕ'_s, but not to ϕ'_c. In any event an unknown quantity is introduced which will produce an error of an unknown amount in the correlation measurement. For this reason, the reactor power must remain constant during the three to five cycles of oscillation while correlation data is accumulated.

REFERENCES

1. Z. Akcosu, "General Solution of the Kinetic Equation Without Feedback," Nuclear Science and Engineering, Vol 3, No. 4 (1958)

2. C. W. Griffin and J. G. Lundholm, Jr., "Calibration of the SRE Control Rods by the Oscillation Technique," NAA-SR-3764

3. C. Starr and R. W. Dickinson, Sodium Graphite Reactors, Addison-Wesley (1958)

4. C. W. Griffin and J. G. Lundholm, Jr., "Measurement of the SRE Power Coefficients and Reactor Parameters Utilizing the Oscillator Technique," NAA-SR-3763

5. C. W. Griffin and J. G. Lundholm, Jr., "Measurement of SRE and KEWB Prompt Neutron Lifetime Using Random Noise and Reactor Oscillation Techniques," NAA-SR-3765 (October 15, 1959)

6. P. E. A. Cowley, "The Application of an Analog Computer to the Measurement of Process Dynamics," Paper 56-IRD-20, ASME (September, 1956)